ABSTRACT

Title of thesis: DEVELOPMENT OF AN ADDITIVELY MANUFACTURED RIGID SPACESUIT COMPONENT FOR LONG DURATION MISSIONS

Team SPACE: Harrison Bartlett, Joseph Bowser, Carlos Callejon Hierro, Sarah Garner, Lawrence Guloy, Christina Hnatov, Jonathan Kalman, Baram Sosis

Thesis directed by: Dr. David Akin
Department of Aerospace Engineering

Long duration human exploration of Mars will pose demands on spacesuits that current designs are unable to overcome, including the need for in-situ replacement and repair of suit components. Advancements in additive manufacturing (AM) technologies provide capabilities to repair or replace rigid pressure garments on-site and on-need. This thesis focuses on a potential application for in-situ hard suit manufacturing: the integration of AM components into a functional spacesuit arm. Material tests were conducted and top candidates were selected for the joint segment components. AM bearing configurations were tested under operational loads and seals were incorporated for pressure retention. Selected components were integrated into a hard suit arm, which was compared to the Shuttle-era EMU arm through human tests in a pressurized glove-box. The results indicate that further refinement of hard suits has the potential to match the performance of operational EMU models while reducing the logistical issues with current spacesuits.

DEVELOPMENT OF AN ADDITIVELY MANUFACTURED RIGID SPACESUIT COMPONENT FOR LONG DURATION MISSIONS

by

Harrison Bartlett, Joseph Bowser, Carlos Callejon Hierro,
Sarah Garner, Lawrence Guloy, Christina Hnatov,
Jonathan Kalman, Baram Sosis

Thesis submitted in partial fulfillment of the requirements of the
Gemstone Honors Program, University of Maryland, 2019

Advisory Committee:
Dr. David Akin, Advisor
Dr. Andrew Becnel, Discussant
Dr. Mary Bowden, Discussant
Lemuel Carpenter, Discussant
Andrew Lamont, Discussant
Michael Restaino, Discussant

Acknowledgments

We would like to offer an enormous thank you to Dr. David Akin for his guidance and support throughout this four-year process, we could not have done it without him! Additionally, we would like to thank Dr. Mary Bowden, Dr. Andrew Becnel, Lemuel Carpenter, Andrew Lamont, and Michael Restaino for serving as discussants for our thesis. Lemuel Carpenter and Dr. Andrew Becnel also provided us with advice and assistance that we are extremely grateful for. Thank you also to Dr. Sarah Over and Elizabeth Soergel for their guidance as our team librarians. We would also like to acknowledge Tracie Prater and the NASA personnel who provided us with support throughout the 2017 X-Hab Academic Challenge. Finally, we would like to thank the Gemstone Honors Program staff - Dr. Frank Coale, Dr. Kristan Skendall, Dr. Vickie Hill, Leah Tobin, and Jessica Lee - for providing the opportunity to engage in an extensive interdisciplinary research project as undergraduate students.

Table of Contents

Acknowledgements ii

List of Tables v

List of Figures vi

List of Abbreviations viii

1 Introduction 1

2 Literature Review 4
- 2.1 Overview . . . 4
- 2.2 Current Spacesuits . . . 4
  - 2.2.1 Overview . . . 4
  - 2.2.2 The Extravehicular Mobility Unit (EMU) . . . 5
  - 2.2.3 Layers of the EMU . . . 6
  - 2.2.4 Spacesuit Limitations and Considerations for Future Design . . . 7
- 2.3 Comparison of Soft or Hybrid Suits and Hard Suits . . . 8
  - 2.3.1 Soft and Hybrid Suits . . . 8
  - 2.3.2 Hard Suits . . . 10
- 2.4 3D Printing Materials and Processes . . . 13
  - 2.4.1 Overview . . . 13
  - 2.4.2 Fused Deposition Modeling . . . 13
  - 2.4.3 PolyJet . . . 14
  - 2.4.4 Selective Laser Sintering . . . 14
  - 2.4.5 Direct Metal Laser Sintering . . . 15
- 2.5 Seal Design and Sealing Surfaces . . . 16
  - 2.5.1 Overview . . . 16
  - 2.5.2 Pressure-Energized Lip Seals . . . 16
  - 2.5.3 X-Ring Seals . . . 17
- 2.6 Conclusion . . . 18

3 In-Situ Fabricated Space Suits for Extended Exploration and Settlement 20
3.1 Joint Design . . . 20
3.2 Material Properties Testing . . . 22
3.2.1 Tension Tests . . . 23
3.2.2 Hydrostatic Tests . . . 27
3.2.3 Discussion of Results . . . 30

4 Developing Technologies and Techniques for Additive Manufacturing of Spacesuit Bearings and Seals 31
4.1 Preliminary Pressure Testing and Seal Design . . . 31
4.1.1 Glovebox Test Procedure . . . 31
4.1.2 Design Iteration One: Pressure Energized Lip Seal . . . 32
4.1.3 Design Iteration Two: X-Ring Seal . . . 36
4.2 Leak Rate Quantification . . . 40

5 Development and Testing of a 3D-Printed Spacesuit Elbow Assembly 43
5.1 Existing Research . . . 43
5.1.1 Kinematics . . . 43
5.1.2 Seal Development . . . 44
5.2 Finalized PHASE Design . . . 45
5.2.1 Additional Seal Testing . . . 45
5.2.2 Interfaces . . . 47
5.2.2.1 Upper Arm - UMd Glovebox . . . 47
5.2.2.2 Forearm - EMU Wrist Disconnect . . . 49
5.2.3 Pressurized Glove . . . 50
5.2.4 Final Assembly . . . 51
5.3 Design Evaluation . . . 53
5.3.1 Timed Task Completion Testing . . . 53
5.3.2 Comfort Testing . . . 55
5.3.3 Participant Selection . . . 56
5.4 Discussion of Results . . . 56
5.4.1 Fitts Tapping Test . . . 56
5.4.2 Elapsed Time Analysis . . . 59
5.4.3 Participant Surveys . . . 61
5.4.4 Sources of Error . . . 64
5.5 Future Work . . . 65
5.6 Conclusion . . . 67

6 Final Discussion 69

Bibliography 71

List of Tables

3.1 Tensile test results: tensile strengths. 24
3.2 Hydrostatic Test Results and Observations 28
3.3 Hydrostatic Test Results Hoop and Axial Stresses 30

4.1 Glovebox Test Results using Design Iteration One 34
4.2 Glovebox Test Results using Design Iteration Two 38
4.3 Leak Quantification Test Results (Glovebox Tests Trials 7-12) 41

List of Figures

1.1 EVA hours over time . . . 2

2.1 Diagram of spacesuit components . . . 5
2.2 Layers in the EMU . . . 7
2.3 Shuttle-era upper arm convolute joint . . . 9
2.4 AX-5 hard-joint design . . . 11
2.5 Pressure energized lip seal . . . 17
2.6 X-ring seal . . . 18

3.1 CAD assembly of prototype . . . 21
3.2 PHASE outer and inner wedges . . . 21
3.3 Bearing assembly . . . 22
3.4 Cross sections of wedges with lip seal . . . 22
3.5 Stress-strain curves of PLA . . . 24
3.6 PLA failure modes . . . 25
3.7 Stress-strain curves of RGD840 Veroblue . . . 26
3.8 Pressure vessel made of PLA . . . 27

4.1 Bearing fitted into SSL glovebox . . . 32
4.2 CAD of PHASE with lip seal . . . 33
4.3 Lip seal following glovebox test . . . 35
4.4 Bearing race failure . . . 36
4.5 X-Ring seal integrated onto an inner race . . . 37
4.6 X-Ring seal integrated into the PHASE bearings . . . 39

5.1 CAD model of the PHASE prototype . . . 44
5.2 Cross sectional view of the PHASE sealed bearing design . . . 45
5.3 Bearing design with aluminum sealing surface . . . 46
5.4 Finalized arm interfaces . . . 48
5.5 EMU wrist disconnect . . . 50
5.6 Picture of assembled glove . . . 51
5.7 Picture of assembled arm . . . 53
5.8 Fitts Reciprocal Tapping Test board . . . 54
5.9 Scatter plots of Fitts Test data . . . 57

5.10 Linear regressions for Fitts Test 58
5.11 Normalized time required to complete one test 59
5.12 Normalized time required to complete a test at a given Index of Difficulty 60
5.13 Average responses to questionnaire (positive) 61
5.14 Average responses to questionnaire (negative) 62
5.15 Average scores on NASA's Task Load Index 63
5.16 Average responses regarding perceived success 63
5.17 Average Cooper-Harper Handling Quality flowchart scores 64

List of Abbreviations

ABS	Acrylonitrile Butadiene Styrene
AM	Additive Manufacturing
AX-5	Ames Experimental Suit 5
CAD	Computer-aided Design
DMLS	Direct Metal Laser Sintering
EMU	Extravehicular Mobility Unit
EVA	Extravehicular Activity
FDM	Fused Deposition Modeling
HUT	Hard Upper Torso
LCVG	Liquid Cooling and Ventilation Garment
ISS	International Space Station
NASA	National Aeronautics and Space Administration
PHASE	Printed Hard Arm Spacesuit Enhancement
PLA	Polylactic Acid
PLSS	Primary Life Support System
ROM	Range of Motion
SLS	Selective Laser Sintering
SPACE	Spacesuit Prototype to Augment Capabilities on EVA
TMG	Thermal Micrometeoroid Garment

Chapter 1: Introduction

It has been over 50 years since the first human ventured outside the protective walls of a spacecraft and into the vacuum of space. Since that historic first extravehicular activity (EVA), humans have logged over 1,000 EVA hours [1]. The EVA, or spacewalk as it is colloquially known, has since taken on a major role in human space exploration, with cumulative EVA hours increasing exponentially from the first spacewalk in 1965 (Figure 1.1). EVAs allow astronauts to accomplish a wide variety of tasks, from the geological studies conducted on the lunar surface during the Apollo missions to maintenance and repair work on the International Space Station (ISS) and Hubble Space Telescope [1].

To keep astronauts safe while performing EVAs, spacesuits must provide adequate protection from the hazards of space. Potential threats to the astronaut that must be considered include extreme changes in temperature, micrometeoroid impact, radiation, suit pressurization, and loads applied to the suit while completing tasks on EVA [2]. A typical spacesuit, therefore, must contain many different layers to provide cooling, pressurization, and protection from the external environment. Each layer of protection, however, comes at the cost of restricting the astronauts ability to move to some degree. The most problematic of these are the layers that

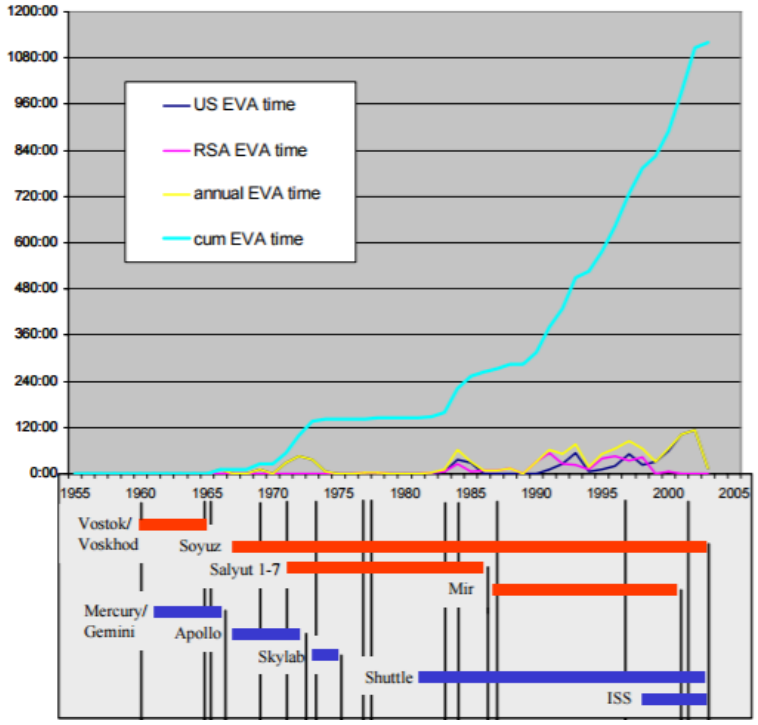

Figure 1.1: Illustration of EVA hours over time, showing various U.S. and Soviet/Russian programs [1]. Dark blue, pink, and yellow lines provide annual data, light blue represents cumulative EVA time.

provide pressurization, as soft pressure envelopes exhibit elastic properties in a vacuum, which cause them to resist bending [3].

Already, significant progress has been made in combating the loss of mobility caused by suit pressurization. During the first spacewalk in 1965, Alexei Leonov wore a suit that was not designed to promote mobility, resulting in the inability to move his fingers. He was only able to re-enter the spacecraft after partially deflating his suit to reduce the pressure differential [4]. For the first American EVA later that year, Edward White wore a suit similar to an inner tube tire. The suit featured a layer of netting slightly smaller than the pressure layer it covered to prevent the expansion suffered by Leonov and promote mobility [1]. This design,

incorporating what is known as a restraint layer, became the standard of spacesuit design through the present. The addition of features like rolling convolute joints and rotating bearings helped to further reduce the change in volume of the pressure envelope during movement, further improving mobility [1].

Additive manufacturing (AM) (or 3D printing) can be used to create a hard spacesuit that can be used on long-distance, long-duration, and potentially open-ended Mars exploration and settlement missions. This suit will not only weigh significantly less, but will increase astronauts' mobility and their ability to work. Furthermore, the use of additive manufacturing will allow the suit to be easily and cheaply repaired or replaced while in space, enabling longer-duration missions than would otherwise be possible. The goal for this project, then, was to determine whether a rigid-element spacesuit can be constructed using additive manufacturing that will improve on current state-of-the-art spacesuit design. The research question addressed is: Can a 3D-printed hard suit be created that has at least as much maneuverability as current (soft or hybrid) spacesuits but at a lower weight?

Chapter 2: Literature Review

2.1 Overview

This section describes the current research on spacesuit design as it applies to the project. A general background on the basic principles of spacesuit design, a comparison between different types of spacesuits, and an overview seals are used in spacesuit design are presented. Current literature on spacesuit design supports the claim that a 3D-printed hard suit can improve on current spacesuits.

2.2 Current Spacesuits

2.2.1 Overview

This section reviews basic spacesuit functions, anatomy, and design requirements currently in use by NASA. Although there are three different types of spacesuits, the focus will primarily be on EVA suits – those used for planetary exploration and spacewalks – as these are the kind we intend to improve upon.

2.2.2 The Extravehicular Mobility Unit (EMU)

An EVA suit protects the human body from the severe conditions of outer space, keeping astronauts safe from the extreme temperatures, radiation, and vacuum to which they are exposed during EVAs. The spacesuit currently in use by the ISS is the EMU [2]. The EMU provides the following functions, among others: pressure retention, oxygen pressure regulation, atmosphere revitalization (CO_2 removal), temperature control, and radiation protection [5]. It consists of several parts, displayed in Figure 2.1.

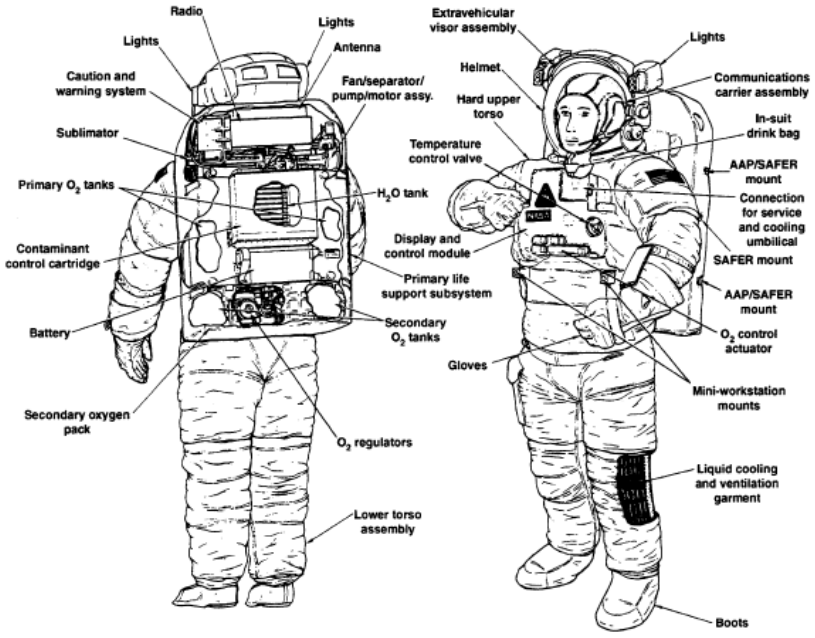

Figure 2.1: Diagram showing the many small but necessary components that make up a spacesuit [2].

The helmet's Extravehicular Visor Assembly, comprised of a clear, polycarbonate bubble and visors, protects the wearer from sun and impact. This helmet connects to the Hard Upper Torso (HUT), a shell that covers the chest and serves

as the main structural support for other elements of the EMU. The arm assembly is attached at both shoulders to the HUT and contains two mobility bearings, one at the shoulder and one at the wrist. The bottom half of the EMU is the Lower Torso Assembly and covers the astronaut's legs and feet. The Primary Life Support Subsystem (PLSS) on the back of the spacesuit connects to the HUT, providing power, oxygen, and water for temperature control [2]. The EMU consists of 14 different layers in three assemblies that will be discussed in detail in the following section.

2.2.3 Layers of the EMU

The EMU's layer assemblies, illustrated in Figure 2.2, perform three main functions: temperature control, pressure regulation, and protection from space particles and radiation [6]. Each of these layers keeps the crew member safe by creating conditions inside the suit similar to those on Earth through temperature and pressure regulation.

The innermost layer assembly is the Liquid Cooling and Ventilation Garment (LCVG). The LCVG is a tight-fitting bodysuit with flexible tubing that circulates cold water, removing excess body heat to maintain a comfortable temperature. It contains larger tubes that transport the suit's oxygen back to the PLSS for purification. The second layer assembly is the pressure garment bladder, which enclosses and maintains the suit's atmosphere. The pressure bladder maintains an O_2 partial pressure comparable to that of the Earth's atmosphere [7]. A pressure garment cover made of polyurethane-coated nylon works to keep it in place. The third layer

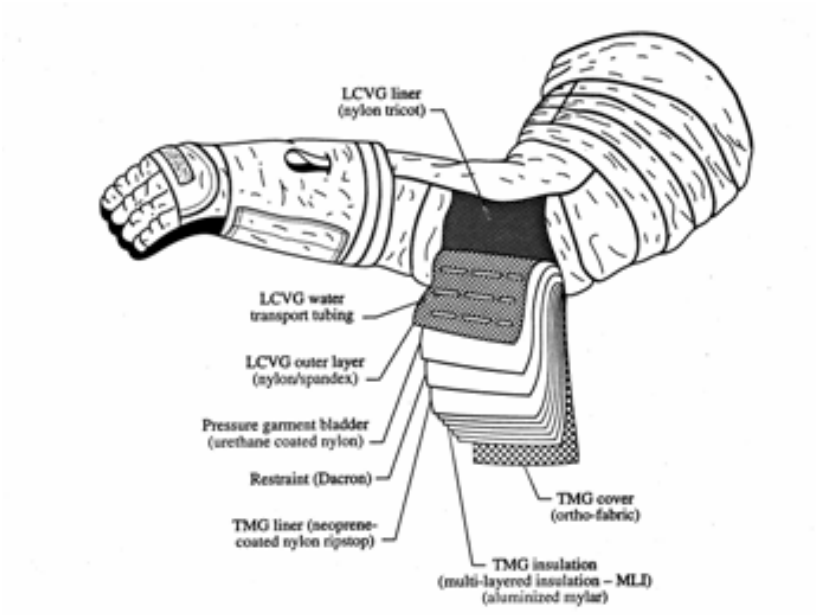

Figure 2.2: Detailed depiction of the many different layers inside the LCVG, Pressure Bladder, and the TMG [6].

assembly is called the Thermal Micrometeoroid Garment (TMG) and consists of a rip-resistant material, thermal layers, and an outermost layer. Space particles traveling at high speeds can potentially rip the suit and harm the astronaut. The micrometeoroid garment layer blocks incoming micrometeoroids and spreads the impact to avoid puncturing the pressure garment. Additionally, the micrometeoroid garment reduces the astronaut's exposure to nominal levels of solar radiation. The thermal layers serve to keep the suit at a comfortable temperature so that the astronaut does not experience the extreme conditions of space [2].

2.2.4 Spacesuit Limitations and Considerations for Future Design

Although the multiple EMU components allow for safe exposure to outer space, their added load and thickness compromise astronaut mobility, causing considerable

fatigue during EVA. As human operations in space increase in frequency and complexity, the need to provide "shirtsleeve" mobility and reduce the strain associated with repetitive physical tasks inside a spacesuit has become a priority for NASA and other organizations pursuing space exploration.

The limited mobility of the EMU causes considerable fatigue for an astronaut during EVA. Areas that experience this sort of fatigue include the thighs, knees and the arms [7]. Currently, 75% of the energy that an astronaut exerts during EVA is spent moving the spacesuit while only 25% is used to perform the required extravehicular task [8]. The metabolic cost of walking nearly doubles in a suit when compared to an unsuited configuration [7]. In addition to fatigue, astronauts often sustain injuries from using the EMU, such as blisters, abrasions, and fingernail delamination, some of which require surgical repair. Data shows that 45.7% of EVA suit tests resulted in injuries [9]. This presents considerable risk to astronauts who may have limited access to medical care.

2.3 Comparison of Soft or Hybrid Suits and Hard Suits

2.3.1 Soft and Hybrid Suits

Spacesuit designs can be divided into two basic categories: hard suits and soft or hybrid suits. Since typically hybrid suits employ fabric joints just like those used in fully soft suits, the two types of suit are treated as interchangeable when compared to hard suits. Soft or hybrid suits have been flown on missions from the Apollo era to the present. As described in Section 2.2.2, these suits are primarily

composed of soft materials and have three main layers: the bladder, restraint, and TMG. The bladder layer serves to maintain a pressurized environment, while the restraint layer bears pressure and loads generated in movement. The outermost TMG layer protects from thermal transfer from space and puncture caused by high velocity microparticles [9].

Soft and hybrid suits must maintain sufficient internal pressure at all times, which limits flexibility. Stiffness and stress can occur at the joints because bending changes internal volume and consequently internal pressure [10]. To minimize this, the EMU uses flat pattern joints formed by sewing fabric pleats to the outer side of the joint, as shown in Figure 2.3. The pleats expand during bending, allowing the suit to maintain nearly constant volume, which reduces workload [11].

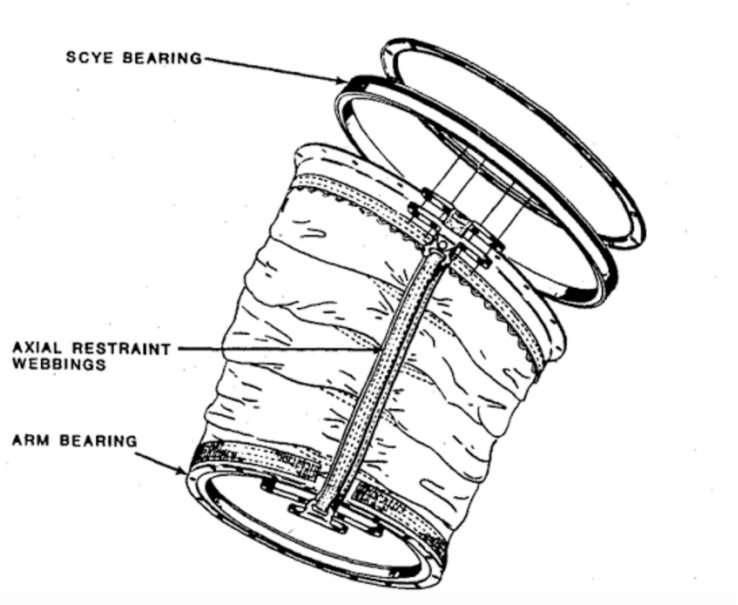

Figure 2.3: Sketch of the upper arm convolute joint from a Shuttle era spacesuit [12].

In flat pattern joints, axial restraints are attached to the sides of a membrane cylinder, several flat gores are connected to enclose the outer side of the joint, and

restraint cables are attached to the enclosure [10]. The restraint cables run down the sides of the arms and legs and bear the axial loads induced by pressurization. They are necessary to prevent the arms and legs of the suit from lengthening when pressurized [11]. If these cables were not present, the gloves and boots of the spacesuit would extend away from the hands and feet under pressure, making most motions impossible.

While the joint architecture of the EMU combats some of the challenges associated with mobility, it has its disadvantages. It is very difficult to bend the joints perpendicular to the axial restraint cables. Flat pattern joints are single-axis joints that do not allow a full range of motion (ROM) in multiple degrees of freedom [11]. Multiple axis bending requires additional rotary bearings in joints such as the shoulders and hips. Additionally, because most work done on an EVA is done in front of the suited person, restraint cables are adjusted so the arms extend forward in a relaxed position rather than outward [11]. This limits the ability of the astronaut to extend the arms outward without causing stress. These restraint cables also make gripping motion more difficult, and can cause fingernail delamination, one of the most commonly reported EVA injuries [9].

2.3.2 Hard Suits

Hard suits have the potential to reduce instances of EVA injury and energy demands on astronauts. Hard suits do not require a bladder layer to maintain a pressurized environment and maintain constant volume, nor do they require axial

restraint cables. They are rigid bodies that use sealed rotary bearings to provide joint articulations.

Hubert Vykukal designed and incorporated such joints into NASA's experimental hard spacesuit design, the Ames Experimental Suit 5 (AX-5) [13]. The elbow joint consists of three serially-connected, truncated, spherical wedges, as shown in Figure 2.4. These wedges rotate against each other to change the angle of the joint [13]. Rotational movement is accomplished using airtight ball bearings at the ends of these sections. The two outer wedges rotate in unison, while the center wedge rotates independently and in the opposite direction [13]. To prevent lock up, a continuous rotable bead chain is integrated into the joint. This allows the outer wedges to track each other in rotation. The design maintains an airtight seal between the suit and the environment while allowing for easy mobility [13].

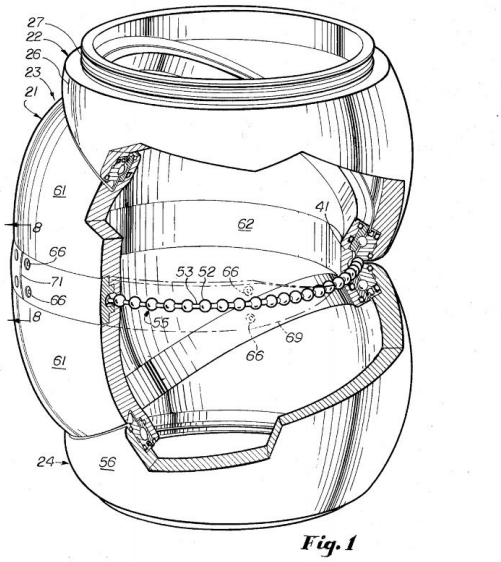

Figure 2.4: Diagram of the hard-joint design used in the AX-5 spacesuit [13].

Though limited data is available on this spacesuit, the AX-5 outperformed soft

and hybrid suits on many quantitative and qualitative tests [14]. This indicates that hard suits have the potential to allow more flexibility and mobility while requiring less torque and energy than soft or hybrid suits.

Despite their potential advantages over current spacesuits, hard suits have some considerable disadvantages. Most significantly, due to their all-metal construction, they occupy more volume and typically weigh more than soft or hybrid suits. This is largely why hard suit designs have never been flown. However, development of a maneuverable and easily fabricated EVA suit is critical for potential future missions to Mars and the Moon. Crew members may have to spend extended periods of time on these missions, from six months to one year on the Moon and fifteen months or more on Mars [14]. The EVA requirements of long duration missions are not compatible with the current method of fabricating spacesuits. Current soft and hybrid suits are crafted by a small number of highly skilled technicians [14]. This means that these suits cannot be repaired in-situ, and require delivery of prefabricated parts, which would be both costly and infeasible in remote locations.

Hard suits may be easier and quicker to fabricate and maintain, making them a viable alternative to current soft or hybrid suits. Innovations in 3D printing technology can assist with fabricating new and replacement parts for hard suits.

2.4 3D Printing Materials and Processes

2.4.1 Overview

Additive manufacturing has become an essential tool in the engineering industry for its ability to turn a computer-aided design (CAD) model into a physical model with relative ease. This technology has facilitated the systems design process by enabling the frequent and inexpensive creation of proof-of-concept models and allowing the production of complex parts that are difficult to manufacture with conventional methods [15]. Particularly in the aerospace industry, 3D printing has proven useful in reducing the cost and complexity of manufacturing components such as air ducts, engine compartments, brackets, suspension parts, and door handles. Unlike traditional subtractive manufacturing methods, such as drilling, cutting, grinding, or forging, additive manufacturing involves an additive, layer-by-layer fusion of the desired material into a desired shape [15]. To print an object with additive manufacturing, a CAD model is converted to a format compatible with the printer, and then fabricated using the desired modeling material and technique. Four main 3D printing techniques are investigated here as they pertain to the spacesuit design effort.

2.4.2 Fused Deposition Modeling

Fused Deposition Modeling (FDM) is a commonly used solid-based additive manufacturing method in which a thermoplastic filament is melted and deposited

onto a bed to create a three-dimensional object. Common FDM materials include polylactic acid (PLA) and acrylonitrile butadiene styrene (ABS). The fabrication process is facilitated using support material that serves as a scaffolding to support a part as it is printed [15]. FDM is a useful prototyping technique as it enables the rapid fabrication of conceptual designs in the preliminary design process. While FDM is widely used for fabricating mock-up designs or performing fit-checks within an assembly, material limitations of FDM thermoplastics make this 3D printing technique unsuitable for aerospace applications which require precision.

2.4.3 PolyJet

PolyJet is an additive manufacturing process commonly used for modeling and prototyping applications which offers high-precision and surface smoothness [16]. This manufacturing technique is unique in that it may be used to create parts with variable rigidity and flexibility using multiple materials simultaneously, as well as achieve ± 0.1 mm tolerances [16]. PolyJet 3D printers deposit droplets of photopolymer resins onto a printing bed, which are cured into three-dimensional objects using UV light [16]. Due to PolyJet's ability to produce high-resolution flexible parts, the process is useful for fabricating O-ring and X-ring bearing seals.

2.4.4 Selective Laser Sintering

Selective Laser Sintering (SLS) is a more sophisticated additive manufacturing technique whereby particulates of plastic, ceramic, or glass are fused by a high-

power laser to create a three-dimensional object. The fabrication process involves distributing a thin layer of a powdered material onto a printing bed and heating it with a laser just below its boiling point, which fuses the powder into a solid. The printing bed then descends slightly, exposing a new layer of powder for the laser to trace and fuse [15]. This additive manufacturing technique is ideal for a range of engineering applications from functional prototyping to small batch manufacturing, and offers ±0.1 mm tolerances [17]. Unlike FDM materials, which have severe material, thermal, and structural limitations, there exist SLS materials which have been certified for spaceflight. A common example is Windform XT, a carbon fiber-reinforced composite 3D printing material used in small satellites and spacecraft components [8].

2.4.5 Direct Metal Laser Sintering

Direct Metal Laser Sintering (DMLS), a sub-category of SLS, is an additive manufacturing technique that uses a high-power laser to melt and fuse a powder, with the added distinction that the powder is metallic. A variety of materials, such as stainless steel, aluminum, or nickel-based alloys, may be used to create functional spacecraft hardware. DMLS printing is suitable to the complex lattice-type geometries and thin-walled structures so commonly found in aerospace components [18]. This paper, however, does not employ DMLS printing as the prohibitive costs associated with it are outside the program budget.

2.5 Seal Design and Sealing Surfaces

2.5.1 Overview

Rigid spacesuits contain airtight rotary seals to allow the elements to rotate while maintaining a livable atmosphere inside the suit [13]. Previous American spacesuits have used two main types of rotary seals – pressure-energized lip seals and X-ring seals [8]. For rigid spacesuits, friction between these elements must be kept low, as the torque required for rotation is only generated by the bending motion of the human body. Seals are responsible for 99% of rotary friction in space suit bearings [19], so their design is highly critical.

2.5.2 Pressure-Energized Lip Seals

Pressure-energized lip seals, as shown in Figure 2.5, use the internal pressure of the suit to press the lip against a smooth sealing surface, resulting in an airtight seal. When engaged, friction is created between the seals and sealing surfaces during rotation, which must be overcome with sufficient torque [13]. This friction is usually minimal because the cross sections of these lip seals have a theoretical single point of contact with the sealing surface. However, such rotary friction can become a problem in locations where torque availability is limited [19]. Additionally, pressure-energized seals have a tendency to leak at low operating pressures which must be overcome to allow for their use in spacesuits [20].

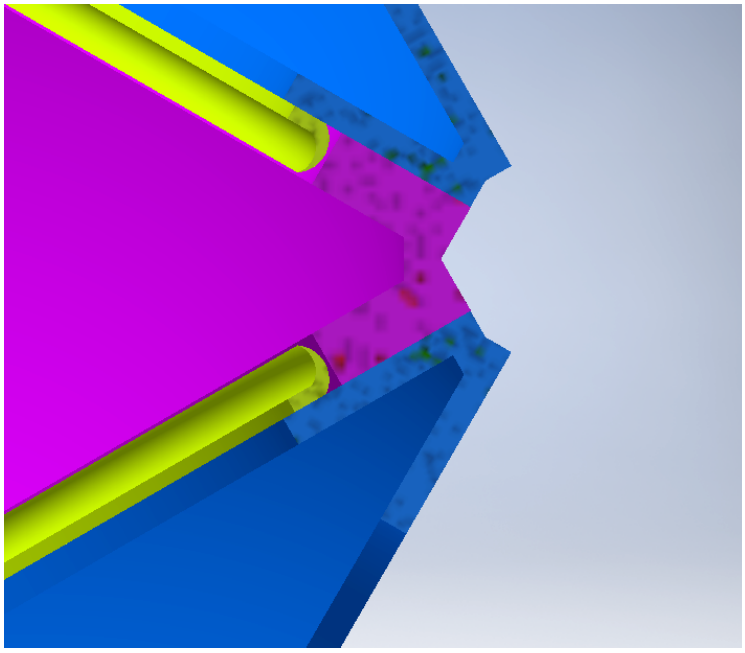

Figure 2.5: A pressure energized lip seal (yellow), attached to one rotary element (blue), is forced against the sealing surface of another rotary element (purple) by the vessel's internal pressure.

2.5.3 X-Ring Seals

X-ring seals are a variation of traditional O-ring seals with a rounded, X-shaped cross section. These seals require less compression than traditional O-rings, reducing the friction they create in rotary applications. X-ring seals theoretically have two points of contact with the rotating sealing surface, which results in a higher theoretical minimum friction than a pressure-energized lip seal. However, this design provides redundancy as the seal will be maintained despite a leak at either point of contact. These seals have been used in various low and high pressure applications. Further research is necessary to determine if 3D printing processes will be capable of meeting the specified tolerances for such seals [21, 22]. An X-ring seal integrated into a rotary bearing is shown in Figure 2.6.

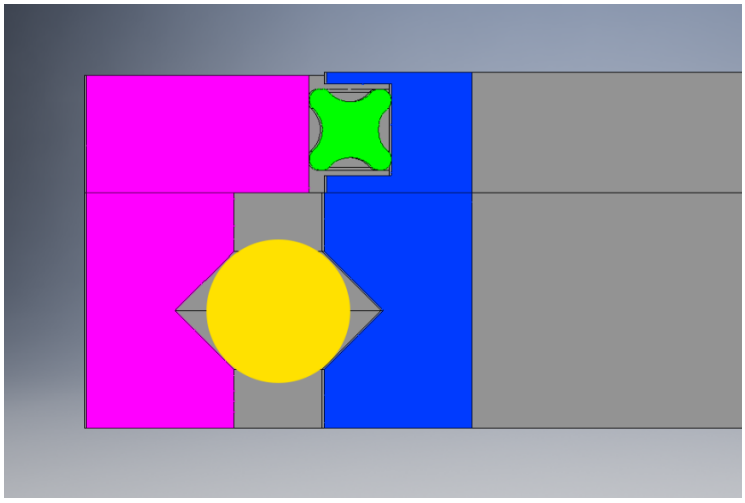

Figure 2.6: An X-ring seal (green) creates an airtight seal between the blue and purple surfaces. The rounded X-shaped cross section and two points of contact are visible.

2.6 Conclusion

The basic soft or hybrid suit design has seen only minor changes since the Apollo program through today. Although the ISS EMU suit offers significant improvements over early suits in terms of mobility and flexibility, it is still far more restrictive than a "shirtsleeve" environment [5]. While metal hard suits have been shown to offer significant improvements in mobility and ROM over modern soft and hybrid suits, they offer additional challenges in increased weight and bulk [14]. These challenges have led to the rejection of these designs in operational spacesuits through the present day.

The development of advanced AM technologies may allow for a new hard suit design that would sufficiently address these concerns. 3D printing allows for the design of a lightweight, modular, hard suit that can be manufactured in-situ rather than on Earth, eliminating the transportation challenges caused by bulkier, heavier

suits.

A wide variety of both quantitative and qualitative tests are required to definitively prove that such a suit is more effective than a traditional soft or hybrid suit, as most individual methods are insufficient by themselves to conclusively compare two suits due to their inherent inaccuracies [23, 24]. The research described above suggests, however, that a hard suit can significantly outperform a traditional soft or hybrid suit in terms of both ROM and energy required for movement.

Chapter 3: In-Situ Fabricated Space Suits for Extended Exploration and Settlement[1]

3.1 Joint Design

The elbow joint was chosen for this project because it serves as a proof of concept because it only has two degrees of freedom and is relatively simple to construct compared to other joints. The joint prototype is based on the design of the AX-5 elbow joint. The joint is constructed of three serially-connected truncated spherical sections. The two outer sections are spheres truncated into right triangular wedges, and the inner section is a sphere truncated into an equilateral triangular wedge. The hypotenuses of the outer wedges meet with the sides of the inner wedge. A CAD model of the prototype is shown in Figure 3.1, and a prototype printed in polylactic acid (PLA) is shown in Figure 3.2.

[1]Published in full in the 47th International Conference on Environmental Systems. Minor revisions are included where appropriate.

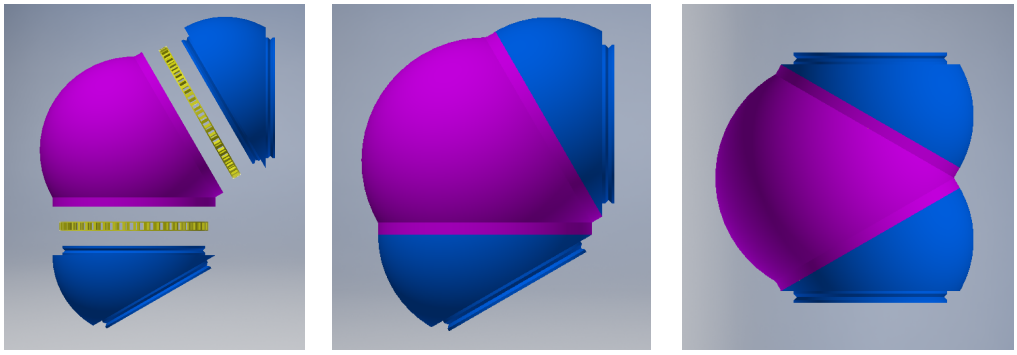

Figure 3.1: CAD assembly of prototype in bent and straightened orientations and with an exploded view.

Figure 3.2: PHASE outer and inner wedges printed using PLA.

The inner angles of the outer wedges are 30 degrees, and the inner angle of the center wedge is 60 degrees. Rotational movement is accomplished using ball bearings integrated into the ends of the wedges, shown without the surrounding wedge elements in Figure 3.3. The outer two wedges rotate together, and the center wedge rotates independently in the opposite direction. When the long sides of the inner and outer wedges are aligned, the sum of the inner angles create a 120-degree bend in the joint. When the long sides of the outer wedges oppose the long side of the inner wedge, the joint is straightened. Inner bearing races are integrated into the ends of the outer wedges, and outer bearing races are integrated into the center wedge. Pressure energized lip seals, shown in Figure 3.4, are attached to the inner

race and seal against the shelf that the outer race sits on.

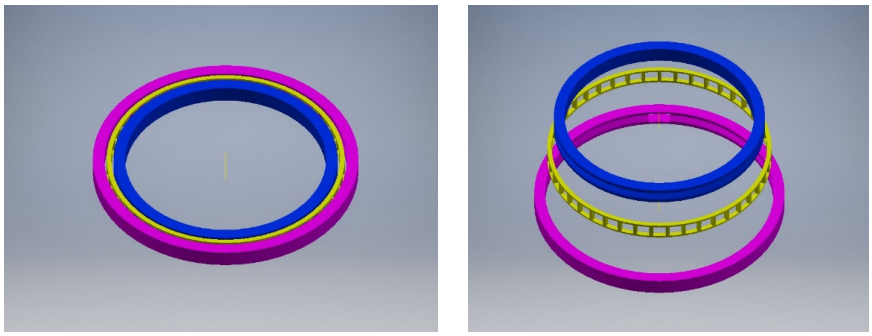

Figure 3.3: Bearing assembly with bearing keeper and exploded view. The inner race (in blue) is integrated into the outer wedges, and the outer race (in violet) is integrated into the inner wedge. Balls not shown.

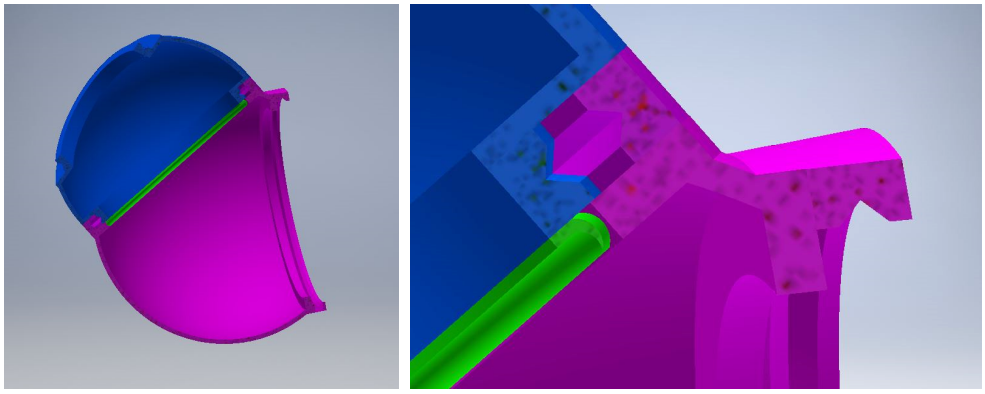

Figure 3.4: Cross sections of inner (blue) and outer (violet) wedge and pressure energized lip seal (green).

3.2 Material Properties Testing

To ensure the structural integrity of the joint, the material properties of different additive manufacturing materials and techniques were evaluated. The primary testing methods were tension tests and hydrostatic tests; these tests were performed to date on PLA and Stratysys' Standard Polyjet Material RGD840 Veroblue. Neither of these materials are certified to use in space, and would not be used in a final

spacesuit design. They were used them here only as prototyping materials to reduce costs, and as such have limited testing to tension and hydrostatic tests. These tests were performed primarily to certify that a prototype made of these materials would be safe to test with human subjects.

3.2.1 Tension Tests

Tension tests were performed on PLA specimens using a hydraulic universal testing machine from MTS Systems Corporation to determine the effects of print orientation on tensile strength. Tests were performed on two groups of test articles: one with a cross sectional area of 0.1875 in^2 (1.20 cm^2) and the other with a cross sectional area of 0.3 in^2 (1.94 cm^2). Furthermore, each group was divided into two subgroups based on print orientation (vertical or horizontal). Specimens printed in a vertical print orientation have strands perpendicular to the long axis, while those printed in a horizontal orientation have strands parallel to the long axis. Stress-strain curves (shown in Figure 3.5) were calculated from the test results using Equations 3.2.1 and 3.2.2. (σ represents stress, F represents force applied, A represents cross-sectional area, ϵ represents strain, δ represents deformation, and L represents initial length.) Average tensile strengths are shown in Table 3.1; the results indicate an average tensile strength of 7150 psi for horizontally-printed specimens and 5230 psi for vertically-printed specimens.

$$\sigma = \frac{F}{A} \tag{3.2.1}$$

$$\epsilon = \frac{\delta}{L} \tag{3.2.2}$$

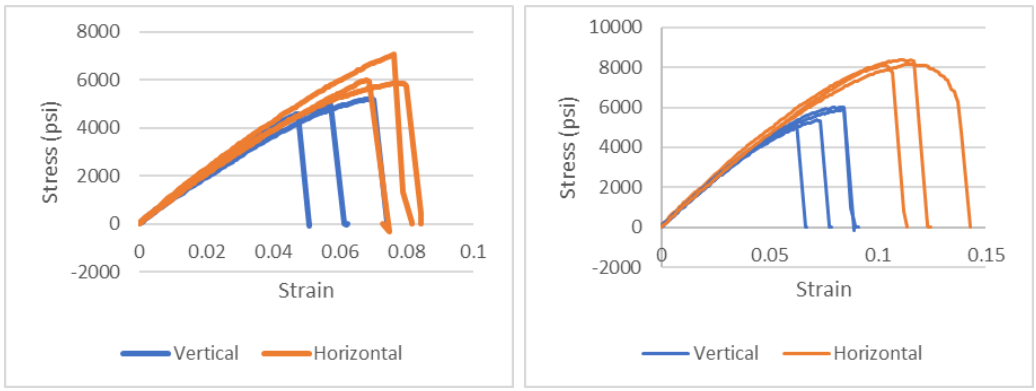

(a) (b)

Figure 3.5: Stress-strain curves of PLA specimens with cross-sectional area of (a) 0.3 in^2 (1.94 cm^2) and (b) 0.1875 in^2 (1.201 cm^2).

Table 3.1: Tensile test results: tensile strengths.

Area / **Orientation**	**0.3 in^2 (1.94 cm^2)**	**0.1875 in^2 (1.201 cm^2)**
Horizontal	6174 psi	8126 psi
Vertical	5027 psi	5446 psi

In both datasets, samples printed with a horizontal orientation show weak signs of yielding or plastic deformation before breaking, acting as a ductile material. Samples printed with a vertical orientation show no sign of yielding or plastic deformation before breaking, acting like a brittle material. Furthermore, samples printed horizontally can withstand a higher maximum stress than those printed vertically. This is because the tensile forces acting on samples printed horizontally act along the layers, rather than perpendicular to them (as they do for samples printed vertically). The high variation in the results is due to the inconsistent quality of

materials printed in PLA. In addition, as shown in Figure 3.6, while most of the specimens broke properly in the center, some 0.3 in^2 horizontal specimens broke on the neck of the specimen, rendering the data from those tests unusable. It would seem this failure mode is caused by a combination of stress concentration at the necks of the specimens and misalignment of the strands at the necks. Although the strands in specimens printed horizontally are generally parallel to the long axis of the specimen, they become less so along the neck due to its outward curve. Thus, the strands in the neck are no longer parallel to the applied tensile forces, causing a weakness in the neck. This explains why no specimens printed vertically showed this failure mode: as there is no difference in strand orientation between the neck and the center of specimens printed vertically, there is less inherent weakness in the neck. The two failure modes are shown in Figure 3.6.

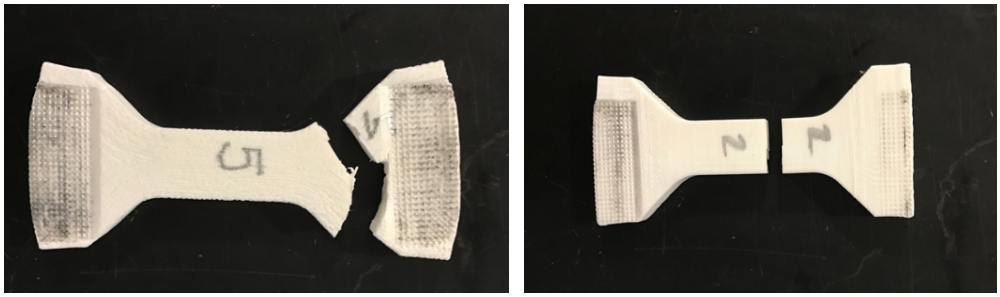

Figure 3.6: Two types of failure modes of PLA specimens.

In addition to performing tests on PLA, tensile tests were also performed on Veroblue specimens created via the Polyjet process. All test specimens have a cross section of 0.0491 in^2 and have a length of 1.5 in. Stress vs. strain curves (shown in Figure 3.7) were produced from tests conducted in the same manner as the PLA tests. There were two groups of tests. The first three tests (as shown in Figure

3.7a) gave inconsistent strain results. Furthermore, the tensile strengths were far lower than that reported in the data published by Stratasys (around 7250-8700 psi). To reconcile these discrepancies, five more tests were performed (shown in Figure 3.7b). Results from these tests match the data published by Stratasys more closely. Specifically, the peak stresses of the first test group ranged from 5173 to 6405 psi, with an error relative to the published data of about 26-31%. Meanwhile, the peak stresses of the second group ranged from ranged from 6110 to 7450 psi with an error of about 14-16%.

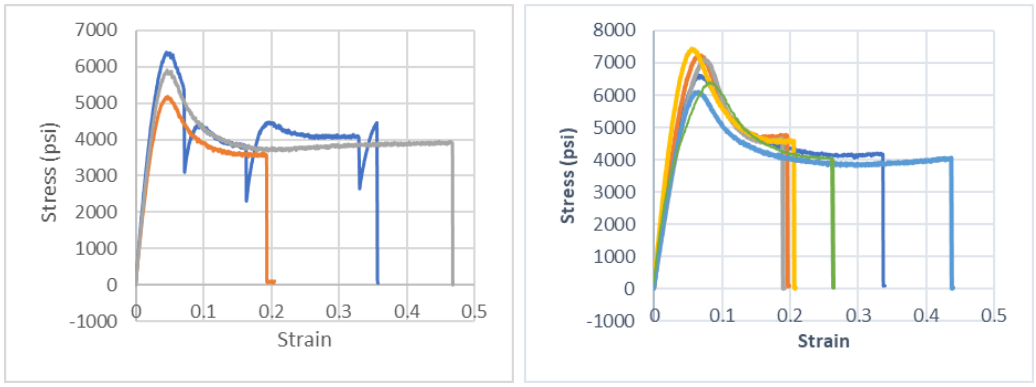

(a) (b)

Figure 3.7: Stress vs. Strain curves of the two different testing groups of RGD840 Veroblue

Based on these experiments, it appears that the Veroblue's ductile behavior caused inconsistencies when these specimens failed. Figures 3.7a and 3.7b demonstrate these inconsistencies by showing multiple points of failure occurring at different strains. Despite these inconsistencies, the material has a sufficiently high peak and yield stress to bear relevant loads, and therefore is a viable material to use in the initial human testing discussed in Section V [in original publication].

3.2.2 Hydrostatic Tests

Hydrostatic tests were also employed to assess material properties. The team's prototype has an operating pressure of 8.3 psi with a safety factor of 3 (resulting in a pressurization requirement of 25 psi); hydrostatic tests verified that chosen 3D printable materials can hold this pressure. Pressure vessels (such as that shown in Figure 3.8) were printed using PLA (with and without an external West Systems epoxy coating) and Veroblue to determine the pressure at which the materials leak and the pressure at which they burst. Vessels were submerged in the University of Maryland Space Systems Laboratory (SSL) neutral buoyancy tank and pressurized until they either burst or the maximum pressure of the pump was reached. Table 3.2 shows the results of this test, and specifies the conditions of each test specimen. (Test 2 is marked as having a "partial" epoxy coating because after the test was completed, patches of uncovered PLA were discovered near the lip of the bottle. It is unclear whether this affected test results.)

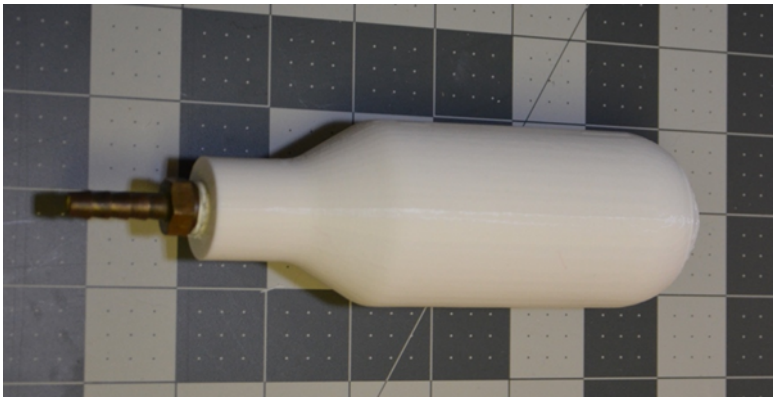

Figure 3.8: A Pressure vessel made of PLA (uncoated).

As shown in Table 3.2, coating the pressure vessels in epoxy significantly im-

Table 3.2: Hydrostatic Test Results and Observations

Test	**Material**	**Wall Thickness**	**Epoxy Coating**	**Pressure at first leak**	**Source of leak**	**Maximum Pressure**	**Cause of test cessation**
1	PLA	1/8 in	None	<1 psi	PLA	N/A	N/A
2	PLA	1/8 in	Partial	90 psi	Inconclusive	100 psi	Hose detached from tap
3	PLA	1/16 in	Full	55 psi	Improperly sealed tap	80 psi	To replace tap
4	PLA	1/16 in	Full	90 psi	Tap	140 psi	Maximum pump pressure
5	Veroblue	1/16 in	None	N/A	N/A	80 psi	Exceeded safety limit
6	Veroblue	1/16 in	None	<1 psi	Crack on the specimen	N/A	N/A
7	Veroblue	1/16 in	None	N/A	N/A	80 psi	Exceeded safety limit
8	Veroblue	1/16 in	None	N/A	N/A	80 psi	Exceeded safety limit

pacts the pressure the vessel can hold. Tests 2-4 demonstrate that when an epoxy coating is used, leaks were observed (if at all) at pressures of 55 psi and up. Meanwhile, with no coating, leaks were observed at less than 1 psi. Furthermore,there were not any violent failure modes: tests 2 and 3 were terminated because of problems with the tap used to secure the pump to the pressure vessel, whereas test 4 was terminated because the maximum pressure of the pump was reached. In no test did the pressure vessel itself burst. Based on these observations, it was concluded that PLA pressure vessels coated with epoxy can withstand a pressure differential of at least 25 psi. Veroblue, on the other hand, can hold pressure without a coating, which makes it a valid material for pressurized parts. The only failure in testing Veroblue occurred due to a crack in the specimen, believed to be due to damage to the specimen before testing. The Veroblue specimens in tests 5, 7, and 8 did not show any signs of failure before exceeding the required safety limit of 80 psi. Based on these observations, Veroblue can withstand a pressure differential of 25

psi without the aid of any coating.

To better quantify the material strength under a hydrostatic test, the pressure data was converted into stress data using Equations 3.2.3 and 3.2.4. (σ_{hoop} and σ_{axial} represent hoop and axial stress, respectively; P represents pressure inside the test specimen; r represents the radius of the specimen; and t represents the thickness of the specimen.) The corresponding hoop and axial stresses are displayed in Table 3.3. Converting the data to hoop and axial stresses allows us to compare the tensile strengths of the materials used in hydrostatic testing to other published data, and to the experimental results. Experiments reported in Section 3.2.1 above found an average tensile strength for PLA of 7150 psi for horizontally-printed specimens and 5240 psi for vertically-printed specimens, both far higher than the maximum hoop and axial stresses exerted in the hydrostatic tests. This is consistent with the results of the hydrostatic tests: while several tests failed due to issues with the tap or pump, none of the PLA test cylinders shattered or fractured. Comparable results were found during hydrostatic tests of Veroblue samples. Stratasys reports a tensile strength for the material of 7250-8700 psi [25], significantly higher than the maximum stresses exerted during hydrostatic testing. This explains why no Veroblue samples failed during testing. (The one cracked sample likely cracked before testing began, as mentioned above.)

$$\sigma_{hoop} = \frac{Pr}{t} \tag{3.2.3}$$

$$\sigma_{axial} = \frac{Pr}{2t} \tag{3.2.4}$$

Table 3.3: Hydrostatic Test Results Hoop and Axial Stresses

Test	**Material**	**Hoop stress at first leak**	**Axial stress at first leak**	**Maximum hoop stress reached**	**Maximum axial stress reached**
1	PLA	<1 psi	<1 psi	N/A	N/A
2	PLA	720 psi	360 psi	800 psi	400 psi
3	PLA	880 psi	440 psi	1280 psi	640 psi
4	PLA	1440 psi	720 psi	2240 psi	1120 psi
5	Veroblue	N/A	N/A	800 psi	400 psi
6	Veroblue	N/A	N/A	800 psi	400 psi
7	Veroblue	<1 psi	<1 psi	N/A	N/A
8	Veroblue	N/A	N/A	800 psi	400 psi

3.2.3 Discussion of Results

Based on these results, it was determined that PLA, due to its low print resolution and inability to hold pressure without a coating, is largely unsuitable for use in the final prototype. However, it can be used as a cheap substitute for more expensive materials when prototyping the static elements of the joint (such as the wedge elements) if pressurization is not needed. As such, future unpressurized tests of the prototype will employ wedge elements made in PLA. Veroblue, on the other hand, can likely be used to construct effective seals due to its high print resolution and ability to hold pressure. (Initial tests of a seal prototype made with Veroblue are discussed in Section IV [in original publication].) While its material properties make it a weak candidate for use in a final prototype, it can be used as an analogue for more expensive materials during design and testing.

Chapter 4: Developing Technologies and Techniques for Additive Manufacturing of Spacesuit Bearings and Seals[1]

4.1 Preliminary Pressure Testing and Seal Design

4.1.1 Glovebox Test Procedure

Sealed bearings were tested in the Space Systems Laboratory glovebox at the University of Maryland. The purpose of these tests was to determine the sealed bearings' ability to withstand a pressure differential of 4.0 psi, and to qualitatively assess the friction in sealed bearings under pressure loads. A pressure differential of 4.0 psi was chosen because it is the maximum pressure differential achievable in the UMd glovebox. The target operating pressure of the PHASE prototype is 8.3 psi.

These tests necessitated the design of a modified version of the standard PHASE bearings that were sized for the glovebox opening and had a solid inner race. Figure 4.1 shows this test set up in the glovebox with the first design iteration. The modified bearing was fitted into a circular opening in the glovebox, and the glovebox was pumped down to create a maximum pressure differential of 4.0 psi.

[1]Published in full in the 48th International Conference on Environmental Systems. Minor revisions are included where appropriate.

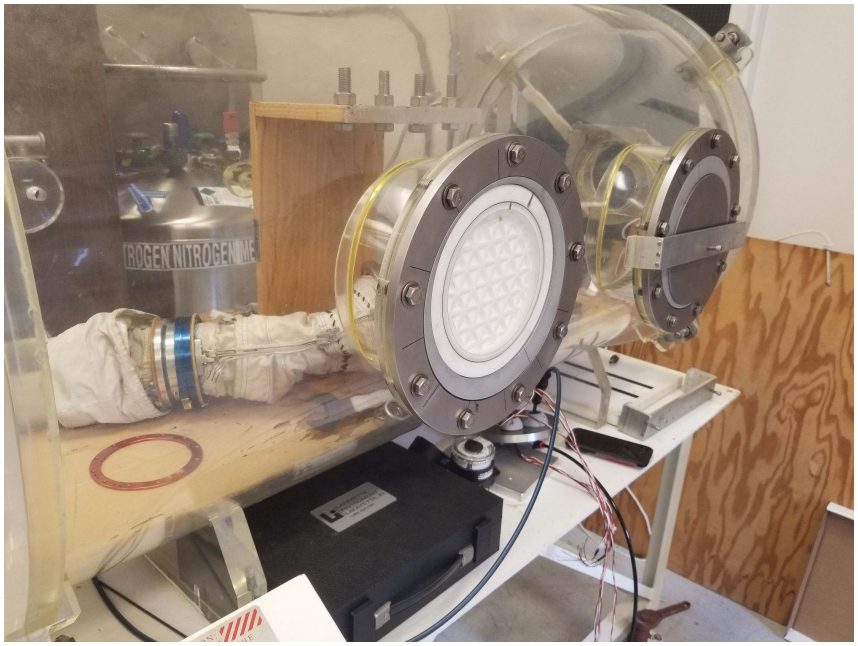

Figure 4.1: Modified bearing fitted into the SSL glovebox for preliminary pressure testing.

4.1.2 Design Iteration One: Pressure Energized Lip Seal

The first seal design evaluated was a pressure energized lip seal that was directly 3D-printed onto the inner bearing race as shown in Figure 4.2a and Figure 4.2b. Note that the modified inner race used for glovebox testing Trials 1 and 2 was printed in Stratasys RGD810 Veroclear material, which has similar material properties as Stratasys RGD840 Veroblue material, based on availability in the laboratory [25].

Lip seals have a theoretical single point of contact with the sealing surface which should have minimized friction and been adequate in withstanding a pressure differential. However, glovebox testing revealed major shortcomings of the design. The contact area between the seal and sealing surface was larger than expected

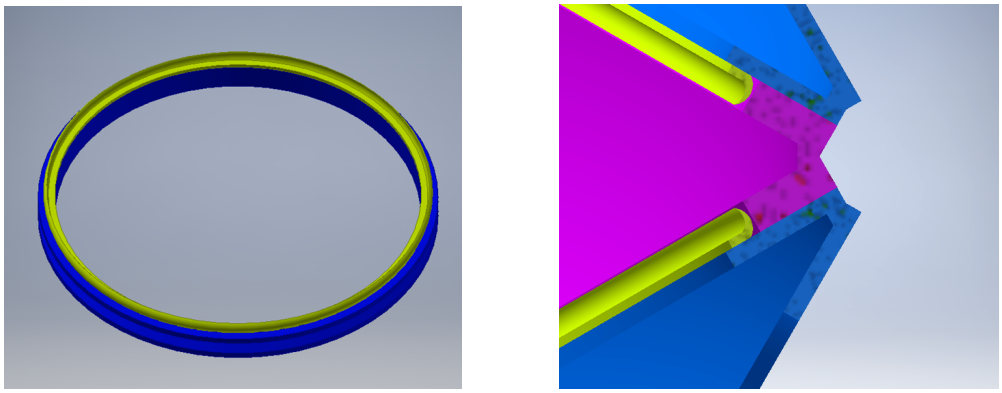

(a) (b)

Figure 4.2: a. CAD of a PHASE inner race (blue) and pressure energized lip seal (yellow) b. CAD cross section of the lip seal (yellow) in a fully assembled prototype. The outer bearing race represented in blue, and the inner bearing race is represented in purple. Note that the actual bearing races are not rendered here.

when pressurized, causing unacceptably high friction. Additionally, since the seal was printed directly onto or otherwise permanently attached to the inner race, it could not be replaced independently. If directly printed onto the inner race, it also needed to be fabricated using a process with multi-material capabilities, such as MultiJet Fusion. The precision required for lip seals was also too high to be resolved using currently available printing processes.

Glovebox testing demonstrated that Iteration One, the 3D-printed lip seal, was not adequate to retain a pressure differential of 4.0 psi. The results of three glovebox tests conducted with the lip seal design are tabulated in Table 4.1.

The lip seal design experienced various different failure modes in glovebox testing that highlighted several of its disadvantages. After each failed test of this sealed bearing design, small corrective adjustments were made to the seal.

Test 1 failed due to improper material choice for the seal. Initial seal designs were fabricated using Stratasys TangoBlack FLX. This rubber-like material was too

Table 4.1: Glovebox Test Results using Design Iteration One

Trial Number	**Seal Material/ Manufacturing Process and Hardness**	**Seal Design and Changes**	**Maximum Pressure Differential (psi)**	**Notes**
1	Stratysys Tango Black FLX (Shore 26-27A)	Lip Seal	2.5	-Seal sucked into gap between races by pressure -Seal was not rigid enough -Material was too soft
2	Stratysys Flexible Digital Material (27A-70A; exact hardness unknown)	Lip Seal -increased material hardness by blending rigid and flexible material -increased lip seal thickness	< 1	-Incorrect sizing of seal -Seal did not have contact with sealing surface
3	Stratysys Flexible Digital Material (27A-70A; exact hardness unknown)	Lip Seal -sizing correction: increasing seal outer diameter to increase contact between seal and sealing surface	3.0	-too much contact with sealing surface -High friction; difficult to rotate -Bearing races began to pull apart -Inner race failed

soft, causing the seal to be overly flexible. As a result, rather than resisting the pressure differential, it was pulled into the gap between the inner and outer bearing races as shown in Figure 4.3.

After observing this failure mode in Trial 1, the thickness of the seal was increased to improve rigidity and fabricated it using a multi-material blend of Stratasys' Polyjet rigid and flexible material, resulting in a harder rubberlike material. However, the exact hardness of this seal material in Trial 2 and 3 is unknown. This is because the campus printing service used to fabricate the seal for these tests did not record the exact ratio of rigid to flexible material.

Test 2 was unable to withstand any pressure differential due to incorrect sizing of the seal. The diameter of the seal was too small, so it did not achieve an adequate sealing pressure. In Test 3, the bearing size was corrected by increasing the outer

Figure 4.3: Lip seal following glovebox test 1. The lip seal was too flexible and was pulled between the inner and outer bearing race by the pressure differential. This prevented the bearing from rotating [26].

diameter of the lip seal by 0.01 inch. This sizing correction made the seal's outer diameter slightly too large, resulting in too much contact with the sealing surface. The increased contact area between the seal and sealing surface created a high level of friction, making the bearing difficult to rotate while pressurized. The pushing force on the inner race required to rotate the bearing cause the races to separate at an angle, which led to destructive failure of the inner race as shown in Figure 4.4.

Tests 2 and 3 revealed a major disadvantage of the lip seal design. Due to the nature of the design, the lip seal sizing required a high level of precision with a tolerance of less than 0.01 inch. Variations in size larger than this were observed to either cause the outer diameter of the seal to be too large to fit inside the sealing surface, or too small to make contact with the sealing surface. This precision and small tolerance is difficult to achieve, and does not allow for slight variation in sizing due to environmental factors, such as humidity, in 3D printing. This, along with the design disadvantages described previously in Section 4.1.2, led to the conclusion that a 3D-printed lip seal would not be suitable for use in the PHASE bearings.

The problems mentioned above may have been able to be mitigated by using a commercially manufactured lip seal, but was not tested in favor of alternative additive manufacturing solutions.

(a) (b)

Figure 4.4: Bearing race began to separate at an angle (left) causing bending forces to act on the inner race. This caused the inner race to fail by breaking in the glovebox (right).

4.1.3 Design Iteration Two: X-Ring Seal

Design Iteration Two used an X-ring seal (Figure 4.5 and Figure 4.6), which mitigated several of the design problems associated with the lip seal. Unlike the lip seal design, this seal did not need to be permanently attached to either of the bearing races. This offered the advantage of independent replacement and easy interchangeability of seals. As shown previously, pressure energized lip seals come to a fine point, making them delicate and therefore difficult to fabricate using 3D printing. The X-ring seal has a more robust design, which helped mitigate these

problems.

The X-ring seal also required significantly less sizing precision than the lip seal. It only needed to be slightly larger in diameter than the groove it fit into so that it would be under compression. The results Trial 4 of glovebox tests using Design Iteration Two indicate that it is capable of withstanding a pressure differential of at least 4.0 psi while rotating easily under pressure loads. The results of these tests are displayed in Table 4.2. Based on these results Design Iteration Two was selected for further testing.

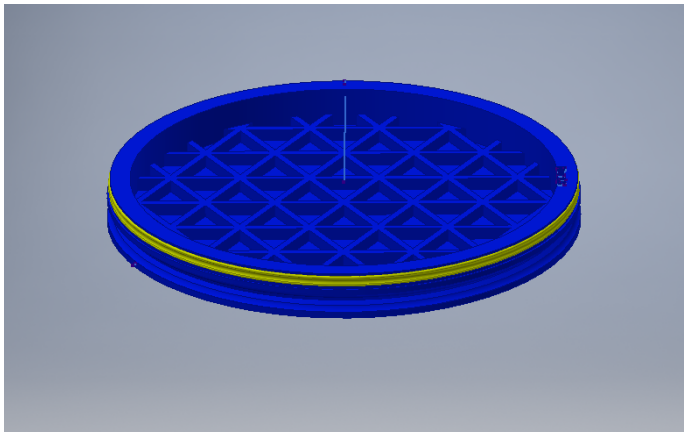

Figure 4.5: CAD of X-Ring seal (yellow) integrated onto a modified solid inner race (blue) used for glovebox testing

Trial 4 was the first test of the X-Ring seal design. As noted in Table 4.2, the bearing races were fabricated of Stratasys' Veroblue material using a Polyjet printing process, and the seal was commercial Viton. In order to attempt to reduce the friction of rotation, the sealing surface on the Veroblue bearing races was smoothed with fine grit sandpaper and the Viton seal was lubricated to reduce friction. The seal withstood the target pressure differential of 4.0 psi and rotated with minimal friction. This test was notable because it was the first successful test of a hybrid

Table 4.2: Glovebox Test Results using Design Iteration Two

Trial Number	**Seal Material/ Manufacturing Process and Hardness**	**Bearing Race Material/ Manufacturing Process**	**Seal Design**	**Maximum Pressure Differential (psi)**	**Notes**
4	Commercial Viton Rubber, Shore 70A	Stratasys Standard Polyjet Material RGD840 Veroblue	X-Ring	4.0	-Successful test -Able to rotate easily -Lubricated seal with high pressure grease -smoothed sealing surface with sandpaper
5	Stratasys Flexible Digital Material, Shore 70A	Stratasys Standard Polyjet Material RGD840 Veroblue	X-Ring	4.0	-Successful test -Able to rotate easily -Lubricated seal with high pressure grease -smoothed sealing surface with sandpaper
6-12	Commercial Viton Rubber, Shore 70A	DuraForm PA**	X-Ring	4.0*	-DuraForm PA (SLS) surfaces are rough -High friciton

* Leaks Observed

** Edited to correct a typo that was left in the original publication

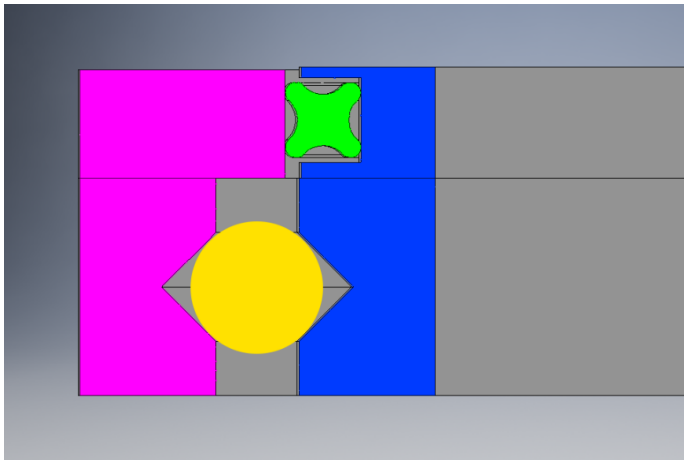

Figure 4.6: CAD cross section of the X-ring seal (green) integrated into the PHASE bearings. The outer race in is in blue, the inner race is in pink, and a ball is in yellow.

3D-printed seal, and determined that the X-ring seal design was suitable for further testing.

Trial 5 was the first test of a fully 3D-printed sealed bearing using the X-ring seal design. As in Trial 1 the seal was lubricated and the Veroblue sealing surface was sanded. All other conditions were also kept constant except that the seal was fabricated of Stratasys Flexible Material using a Polyjet Process. This test was notable because it was the first successful test of a fully 3D-printed spacesuit bearing and seal.

After completing successful tests of both a hybrid and fully 3D-printed sealed bearing using Veroblue races, testing proceeded using DuraForm PA races and commercial X-ring seals. These tests revealed major challenges associated with fabricating sealed bearings from SLS materials. SLS materials have a rough surface finish, which is not ideal for sealing surfaces. This rough surface introduced unacceptably high levels of friction in rotation. Unlike with Polyjet materials, sanding of the

sealing surface did not noticeably improve the surface finish.

Though sealed bearings with DuraForm PA races successfully withstood the target pressure differential of 4.0 psi for all trials, they leaked noticeably. This prompted a change in the original test plan because it was necessary to quantify the severity of the leak in the bearing.

4.2 Leak Rate Quantification

Following Trial 6, a new test procedure was designed to quantify the leak rate of the DuraForm PA sealed bearings. Before Trial 7, vacuum grease was applied on all surfaces where the bearing races interfaced with the glovebox to minimize potential leaks around the bearing edges. As in previous trials, the test bearings were fitted into a circular opening in the glovebox, and the glovebox was pumped down to a maximum pressure differential of 4.0 psi. The measured maximum pressure differential at this point was actually 3.87 psi, which was used to calculate leak rate. After reaching this maximum pressure differential, the glovebox pump was turned off and time required for glovebox to completely depressurize to atmospheric pressure was measured. The results of these tests are shown in Table 4.3.

The results of these trials were used to calculate mass leak rate. This leak rate was calculated as follows:

(1) The volume of the SSL glovebox was calculated the equation below. The main section of the glovebox is a cylinder. Its two rounded end caps were also approximated as cylinders for this calculation. The volume of the glovebox

Table 4.3: Leak Quantification Test Results (Glovebox Tests Trials 7-12)

Trial Number	**Spinning or Static Bearing Races During Depressurization?**	**Time for the Glovebox to Fully Depressurize from 3.87 psi (seconds)**
7	Static	45
8	Spinning	35
9	Static	40
10	Static	43
11	Spinning	36
12	Spinning	34

was found to be approximately 33,200 in^3 or 0.544 m^3.

$$V = \left(\frac{\pi D^2}{4}\right) L_{main\ section} + 2\left(\frac{\pi D^2}{4} L_{end\ caps}\right) \tag{4.2.1}$$

where $L_{main\ section} = 49.75$", $L_{end\ caps} = 7$", and $D = 25.75$".

(2) The number of moles of air in the glovebox at atmospheric pressure (101,320 Pa) and 3.87 psid (74,700 Pa) were then calculated using the ideal gas law. Room temperature (approximately 293 K) was used for calculations.

$$n = \frac{PV}{RT} \tag{4.2.2}$$

where P = pressure [Pa], R = universal gas constant [J/mol-K], V = volume [m^3], and T = temperature [K], which gives $n_{atmospheric} = 22.6$ moles and $n_{3.87\,psid} = 16.67$ moles.

(3) The change in moles, denoted Δn, was then calculated. Using this change in moles, change in mass was calculated using the molecular weight of air, 28.0134 g/mol or 0.06176 lb/mol. Mass leak rate was then calculated by dividing this

leak rate by the average time required for the glovebox to depressurize.

$$\Delta n = n_{atmospheric} - n_{3.87\,psid} = 5.95 \text{ moles} \tag{4.2.3}$$

$$\Delta mass = MW_{air} * \Delta n = 0.3675 \text{ lb} \tag{4.2.4}$$

$$\text{Mass Leak Rate} = \frac{\Delta mass}{t_{average}} = 0.009464 \frac{\text{lb}}{\text{sec}} = 34.07 \frac{\text{lb}}{\text{hr}} \tag{4.2.5}$$

This leak rate is more than 1000 times the acceptable published mass rate for the Apollo Era EMU, 0.0315 $\frac{\text{lb}}{\text{hr}}$ [27]. While it was not actually necessary to perform these calculations to verify that the DuraForm PA sealing surface was unacceptable, it was beneficial to develop the procedure for future testing of design approaches which come closer to flight requirements.

Chapter 5: Development and Testing of a 3D-Printed Spacesuit Elbow Assembly[1]

5.1 Existing Research

5.1.1 Kinematics

This project focuses on the elbow joint due to its utility and relative simplicity. The elbow joint design mimics the kinematics of the AX-5 suit. The Printed Hard Arm Spacesuit Enhancement (PHASE) prototype consists of three wedge elements that are connected through integrated ball bearings. The inner wedge element has a 60 degree angle, while the two outer wedge elements have a 30 degree angle. Arm rotation is achieved by rotating the outer wedge elements around the inner wedge element. A forearm segment allows the prototype to interface with the Extravehicular Mobility Unit (EMU) wrist disconnect, and an upper arm segment allows for integration into the UMd glovebox. A CAD model of the prototype can be seen in Figure 5.1. All components are additively manufactured with the exception of the steel balls inside the rotary bearings, the seals, and the rotary sealing surfaces.

[1]To be published in full later this year in the 49th International Conference on Environmental Systems. Minor revisions are included where appropriate.

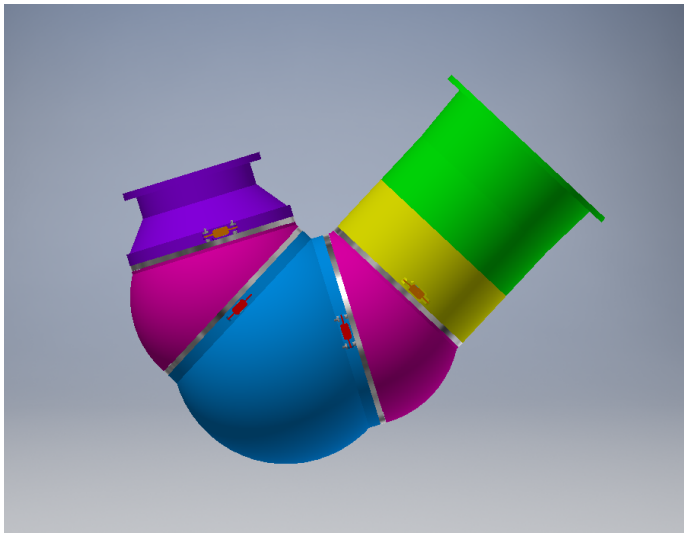

Figure 5.1: CAD model of the PHASE prototype, showing the wrist (purple), outer wedge elements (magenta), inner wedge element (blue), upper arm segments (yellow, green), sealing rings (silver), and bearing plugs (orange).

5.1.2 Seal Development

After testing, it was found that a design using an x-ring seal with races fabricated from DuraForm PA successfully withstood the target pressure differential of 4.3 psi without failure. However, it did not meet minimum performance standards for pressure retention, due to significant leaking and high friction of rotation [28]. A cross-sectional view of this design is shown in Figure 5.2.

Due to the nature of the printing process used for DuraForm PA and other SLS materials, the sealing surface in the bearing was rough and imperfect. Through observations during testing, this was identified as a major cause of friction and leaks.

Additionally, SLS printing processes are only capable of an average precision of ± 0.005 in [29], which is not tight enough to meet the specified tolerances for

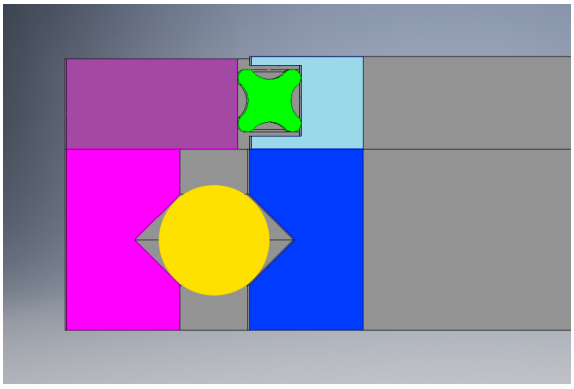

Figure 5.2: Cross sectional view of the sealed bearing design selected for the PHASE prototype. An X-ring seal (green) sits in a groove (light blue) and creates an airtight seal against the sealing surface (purple).The rounded x-shaped cross section and two points of contact are shown. The seal groove and sealing surface are attached and rotate with the inner race (blue) and outer race (pink) respectively.

rotary seals [21, 22]. Due to this, variations between prints can result in interfaces with either too large or too small of a gap between the seal and sealing surface. A gap that is too large does not provide an adequate seal, which can cause leaks between the seal and sealing surface. On the other hand, a gap that is too small creates excessive squeeze on the seal, which increases friction. In tests, this issue was identified as a potential source of high friction.

5.2 Finalized PHASE Design

5.2.1 Additional Seal Testing

After identifying the roughness of the DuraForm PA sealing surface as a potential source of the high leak rates and high friction of rotation observed in bearing tests, three potential methods were investigated to mitigate this issue.

First, vacuum grease was applied to the seals and sealing surfaces to reduce

friction between them. Qualitatively, this led to a small decrease in friction. This reduction in friction was not judged to be sufficient for use in the prototype, however.

The second solution investigated was to coat the DuraForm PA sealing surface with epoxy and then sand it to create a smoother surface. The coated surface was only marginally smoother than the uncoated DuraForm PA surface. In testing no notable difference was observed in leak rate or a substantial decrease in friction of rotation.

Additionally, this solution does not mitigate potential problems related to the precision of the SLS printing process. The increase in friction observed was likely due to the addition of the epoxy coating reducing the effective inner diameter of the sealing ring, thereby increasing the pressure on the X-ring seals. The application and sanding of the epoxy coating is an imprecise process and the SLS printing process itself was already outside of the required tolerances. Therefore, it would have been extremely challenging to size the sealing surface appropriately using this solution.

Another solution that was investigated was replacing the DuraForm sealing surface, shown in purple in Figure 5.2, with a smooth aluminum ring. This design is shown in Figure 5.3.

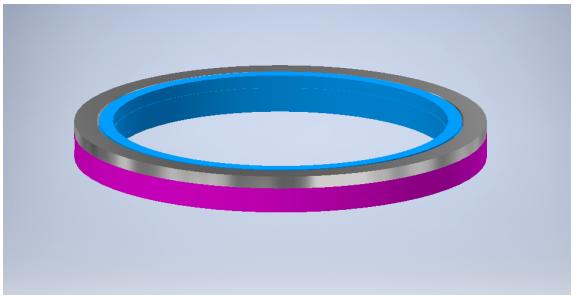

Figure 5.3: CAD rendering of bearing design with aluminum sealing surface (silver). This sealing surface is attached to the outer bearing race (pink).

This method solved issues related to the precision of the SLS printing process, as well as issues related to the roughness of the DuraForm PA. An inner race was initially printed, as shown in blue in Figure 5.2, and the outer diameter of the sealing groove, shown in light blue in Figure 5.2, was measured. Based on this measurement, the aluminum ring was sized appropriately using tolerances recommended for rotary seals [21, 22]. The aluminum ring was then glued on to the outer race, shown in purple in Figure 5.2. In testing, this design demonstrated the ability to retain pressure without significant observable leakage and to rotate with an acceptable level of friction. This design, however, introduces a considerable number of non-additively manufactured components into the design of a full suit. In order to maximize additive manufacturing, the aluminum components in Figure 5.2 were replicated in Veroblue, which was successfully used in prior sealed bearing tests [28]. Based on these results, Veroblue sealing rings were incorporated into the final PHASE design, which was compared to the EMU. This decision, however, was not without its own challenges. While Veroblue test bearings did successfully seal in the glovebox, the process's tolerances still lead to instances of ill-fitting sealing surfaces, which could cause high friction or leakage.

5.2.2 Interfaces

5.2.2.1 Upper Arm - UMd Glovebox

The PHASE arm is designed for evaluation in the UMd glovebox, a differential pressure test chamber capable of achieving 4.3 psid. Due to the dimensions of the

PHASE elbow, the full arm is unable to fit through the glovebox arm port. The upper arm assembly, therefore, consists of two modules: an upper segment that is inserted through the glovebox port, and a lower segment, attached to the elbow wedge elements, that connects to the upper segment. To connect the PHASE arm to the upper arm upper segment, the arm is inserted through the larger side door of the glovebox, as shown in Figure 5.4. The upper segment is inserted through the glovebox port, and four toggle clamps are used to fasten the segments together. The lower segment of the upper arm contains an O-ring to ensure a good seal between the two segments. An operational suit would use additional wedge elements and rotary bearings, as in the PHASE elbow, to connect the upper arm and shoulder to the torso.

(a) (b)

Figure 5.4: Finalized arm interfaces. (a) Photograph of the PHASE arm separated into two upper arm segments (b) Picture of integrated arm in the glovebox port, as viewed from inside the glovebox.

5.2.2.2 Forearm - EMU Wrist Disconnect

The forearm of the PHASE prototype is designed to interface with the EMU wrist disconnect, allowing it to operate with any glove that is compatible with existing interfaces. On the EMU, a seal between the forearm and wrist disconnect is achieved by tightly pressing the suit's pressure bladder between a metal plate and the disconnect, as shown in Figure 5.5. In a hard suit, this setup is not possible, since pressure retention is accomplished by rigid elements rather than a flexible bladder. The wrist disconnect's built-in O-ring seal can, however, be used to form an airtight seal between the wrist disconnect and a smooth 3D-printed surface. Bolts are used to hold the wrist disconnect and its integrated O-ring seal firmly against the forearm, creating an airtight seal. This setup is similar to what would be used in an operational additively manufactured hard suit.

Due to the size and complicated kinematics of spacesuit gloves, rigid elements are poorly suited for this component of the suit. A traditional soft-goods glove would likely be employed, with a quick disconnect mating it to the suit's rigid forearm.

(a) (b)

Figure 5.5: (a) Closeup of the EMU wrist disconnect. The pressure bladder (yellow) can be seen sealing against the blue metal plate. (b) Picture of forearm with integrated wrist disconnect

.

5.2.3 Pressurized Glove

An airtight glove was fabricated to enable pressurized testing in the glove box, due to the lack of an available EMU glove for the extensive testing planned for this project. The glove consists of a pressure bladder made of silicone rubber inside a commercially available work glove acting as a restraint layer. The pressure bladder was created by applying multiple layers of silicone rubber to a 3D-printed hand model and allowing the material to set before removing it from the model. This technique had been previously used in the SSL to fabricate a glove prototype.

The pressure bladder has a 0.25 in. lip in order to attach to the EMU wrist disconnect and provide a smooth sealing surface. The existing EMU wrist disconnect interface was then used to connect the restraint layer, the pressure bladder, and the wrist disconnect together. During pressurization testing, the glove failed to properly seal. Additional fabric was sewn onto the glove before attaching to the

wrist disconnect to alleviate this issue. Once properly sealed, the glove's restraint layer proved inadequate in preventing the glove from ballooning outward. Tape was applied around the palm and thumb in order to help restrain the glove.

Unlike the EMU glove, this glove must be pressurized in order to don and doff it. The glove successfully retained pressure and demonstrated that silicon rubber molds can be useful for rapidly creating basic glove hardware for glovebox testing.

Figure 5.6: Picture of assembled glove

5.2.4 Final Assembly

The rigid elements for the PHASE arm, wrist disconnect and glovebox interfaces, and bearing keepers were fabricated in DuraForm PA by a printing service. Veroblue sealing rings for each bearing were fabricated on campus at the University of Maryland. The Veroblue rings were designed with an alignment groove to ensure they were aligned precisely with the DuraForm wedge elements. The alignment

groove was filled with cyanoacrylate glue, and the wedge elements were pressed into place to ensure an airtight seal between the Veroblue rings and the DuraForm wedge elements.

After integrating the sealing rings and the wedge elements, off-the-self X-ring seals and Duraform bearing keepers were integrated into the bearings. During this process, a large amount of friction was observed between the X-ring seals and the Veroblue rings. To correct this, the Veroblue rings were wet sanded to create a smooth finish and gradually reduce their inner diameter. This process was repeated until a snug but low-friction fit was achieved. Off-the-shelf steel ball bearings were added to the bearings, securing the wedge elements together.

Toggle clamps were attached to the two segments of the upper arm with epoxy. The EMU wrist disconnect was bolted to the forearm of the PHASE arm, and the O-ring built into the wrist disconnect was used to create a seal. Following the integration of these components, the PHASE arm could be inserted into the glovebox and have a pressurized glove attached for testing. The fully assembled arm is shown in Figure 5.7.

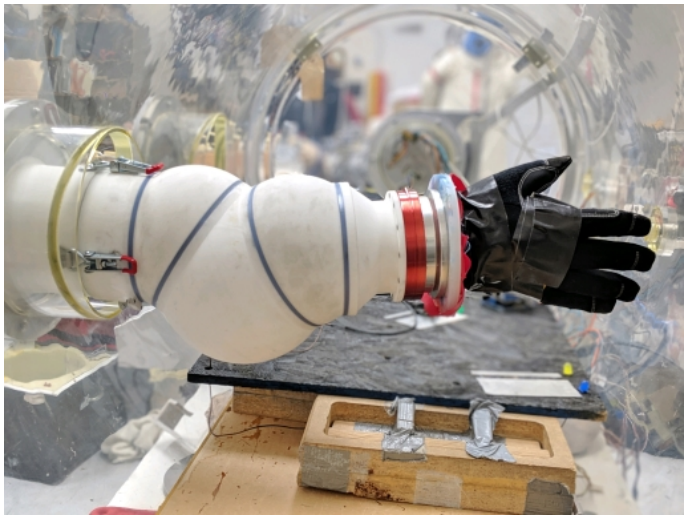

Figure 5.7: Picture of assembled arm

5.3 Design Evaluation

5.3.1 Timed Task Completion Testing

In order to evaluate the performance of the PHASE arm, human subjects were tested to compare it to a Shuttle-era suit arm. Human-subjects testing consisted of both quantitative and qualitative testing. Fitts' Law was used to quantitatively evaluate difficulty of movement while wearing the PHASE arm. Fitts' Law was first published in 1954, and has become a standard in physiological research owing to its robust empirical regularity. The law states that the time required to touch a target is a function of the ratio between the starting distance from the target and the size of the target [30]. In the Fitts Reciprocal Tapping Test, subjects are instructed to repeatedly tap between two plates as fast as possible with a stylus [31]. By instructing the test subjects to minimize their errors while working against a time limit, subjects will naturally adjust the speed of their movement, so that more

difficult movements result in fewer total taps than simpler ones [31]. Fitts' Law describes how to analyze the test results:

$$\mu_T = k_1 + k_2 \times ID \tag{5.3.1}$$

where μ_T is movement time from one target to the next, k_1 and k_2 are constants (in this case dependant on the suit arm used), and ID is the Index of Difficulty [30]. Calculation of ID varies, but is typically a function of D/W, where D is the distance between targets and W is the width of a target [30]. $\log_2(\frac{D}{W})$ is used.

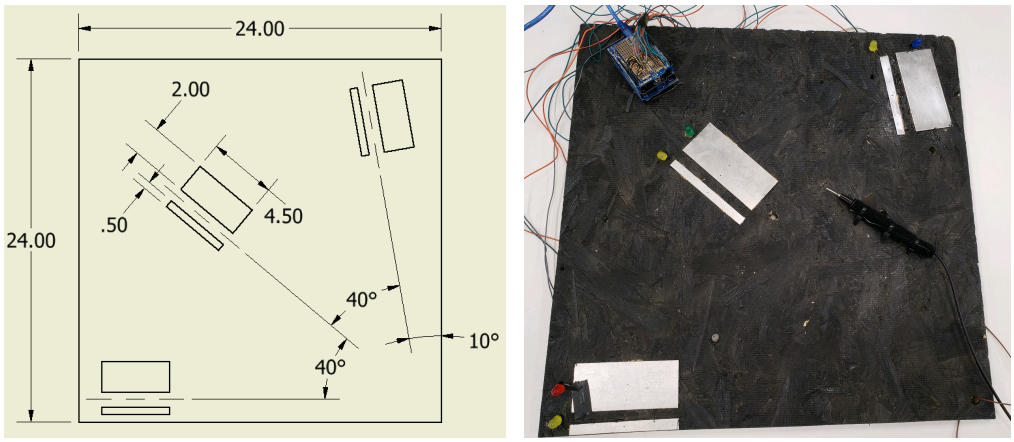

(a) (b)

Figure 5.8: (a) A CAD mockup of the Fitts Reciprocal Tapping Test board. Dimensions are given in inches. (b) Picture of the Fitts Reciprocal Tapping Test board along with the metal stylus used in testing.

The board used to administer the Fitts test is shown in Figure 5.8. The board consists of six metal plates arrayed in pairs along an arc. One plate from each pair is 2 in. wide, while the other is 0.5 in. wide. The three pairs of plates are located at 0, 40, and 80 degrees along the arc. This design allows us to vary both the size of the target (W) as well as the distance between the targets (D) by instructing subjects

to tap between different sets of plates. The subjects undergo a set of six tests per type of arm – EMU pressurized, EMU unpressurized, PHASE unpressurized, and unsuited – over a range of index of difficulties. The total time required to complete ten taps between targets was used for μ_T. A conductive stylus and conductive plates were connected to an Arduino Uno, which was used to measure the tapping times for each participant.

5.3.2 Comfort Testing

Even if a suit provides superior range of motion and requires lower torque for movement than current spacesuits, it will not be effective unless it is comfortable for the astronaut. If a suit rubs against an astronaut's skin, not only will it be uncomfortable to work in, but it can also cause injury during extended-duration EVAs [32]. In several cases, such injuries and discomfort almost led to the termination of an EVA mission [33]. Qualitative comfort feedback is therefore critical to the evaluation of the PHASE design.

Comfort was gauged through a series of questionnaires taken after subjects perform the Fitts Reciprocal Tapping Test. On the first questionnaire, subjects are asked to rate their agreement with statements such as "The arm was comfortable" and "The arm moved the way I wanted it to" on a 6-point Likert scale from "Strongly Disagree" to "Strongly Agree." Subjects then filled out NASA's Task Load Index [34] and a modified Cooper-Harper Handling Quality flowchart [35].

5.3.3 Participant Selection

Participants were recruited through advertisements posted throughout the UMd. campus. Participants were required to be between 5'6" and 6'2" tall, be right-handed, and have a full range of motion in their right arm. These constraints were driven by sizing constraints for the EMU arm available in the SSL. In an effort to minimize the effects of bias and additional experience in the PHASE arm, no members of the research team developing PHASE participated in the trial. In total, 18 participants were recruited.

5.4 Discussion of Results

5.4.1 Fitts Tapping Test

To complete the Fitts' Law analysis, the total times for each trial were calculated, then normalized as a factor of each participant's fastest unsuited trial. These terms were normalized to account for differences in ability between different research participants. These times were then plotted versus Index of Difficulty and fitted to Fitts' Law using linear regression. Following this initial fit, outliers were identified and removed to improve the linear regression. In total, 1 out of 108 unsuited data points, 4 out of 107 PHASE data points, and 1 out of 36 unpressurized EMU data points were excluded from the fit. All of these outliers were uncharacteristically high as compared to other participants at the same Index of Difficulty. A plot of the data for each testing configuration and the linear regressions performed can be

seen in Figure 5.9.

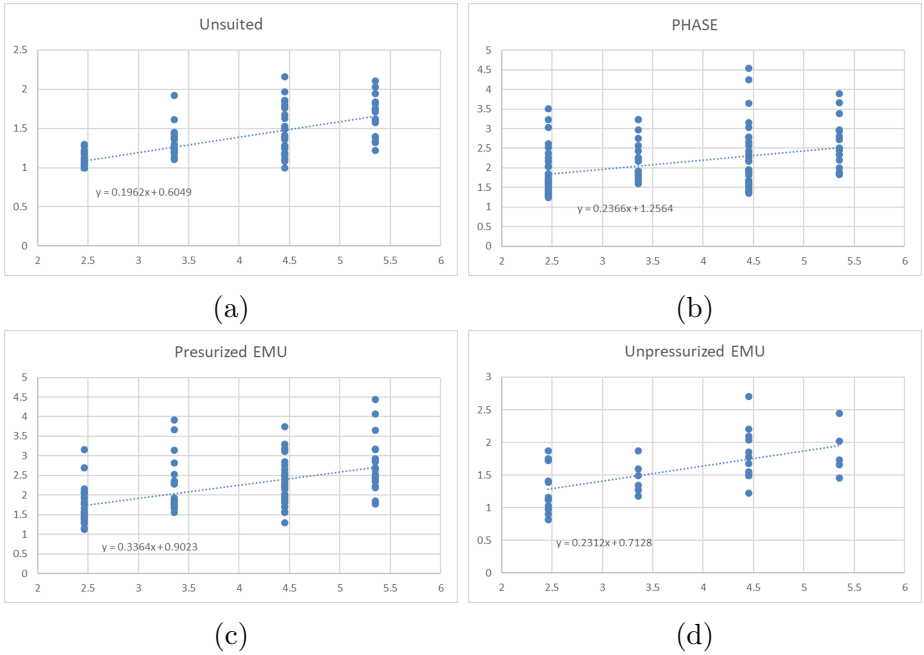

Figure 5.9: Scatter plots of all Fitts Test data for all configurations (clockwise from top left: Unsuited, Unpressurized PHASE, Pressurized EMU, Unpressurized EMU). Linear regressions with Fitts Law constants and R^2 values are also displayed.

Overall, significant spread was observed in the data; however, there were clear clusters of data in enough of the configurations and Indices of Difficultly to allow for the linear regressions to be meaningful. By plotting the resulting linear regressions on top of each other, as in Figure 5.10, the relative difficulty of each configuration can be visualized. At a given Index of Difficulty, points with a higher μ_T correspond to more difficult movement. Thus, a higher y-intercept corresponds to a higher overall difficultly of movement, while a steeper slope indicates that movements become harder more quickly as Index of Difficulty increases.

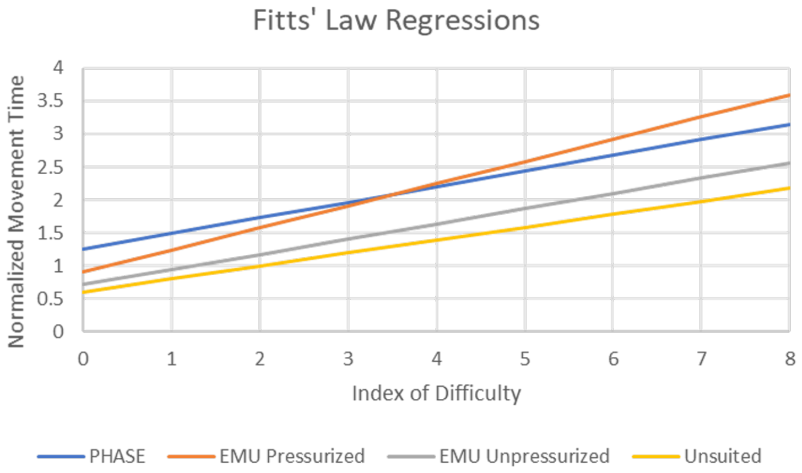

Figure 5.10: Linear regression data for all four test configurations overlaid on one plot.

.

Based on the regressions in Figure 5.10, the unpressurized PHASE arm was overall the most difficult configuration to use, however, the PHASE arm becomes easier to use than the EMU as tasks become more challenging, beginning at an Index of Difficulty of approximately 3.7. This data is consistent with the expectations based on the AX-5 suit. Hard suits require the user to adapt their natural movements to induce rotation into the wedge elements, allowing the suit to bend. Soft suits do not require this adaptation, so for simple tasks, the user will likely find the soft suit easier to use. Pressurized soft suits, however, become more difficult to use the farther they are displaced from their neutral position, and fight the user to return to this position. A rigid element suit does not have a tendency to return to a neutral position, and therefore should be easier to use at higher Indices of Difficulty.

5.4.2 Elapsed Time Analysis

To address concerns that the relatively low R^2 values in the Fitts' Law regressions could be providing inaccurate results, an additional analysis was performed on the total times required for each participant to complete each trial. In this analysis, each of the six tests in the PHASE and pressurized and unpressurized EMU were normalized as a factor of the participant's time completing the same test unsuited. It should be noted that this is a different method of normalization from Subsection 5.4.1. This was done to allow each Index of Difficulty to be analyzed in isolation. The average of these normalized times were computed, both over all trials in each configuration, and for each Index of Difficulty. The results of this analysis can be seen in Figures 5.11 and 5.12.

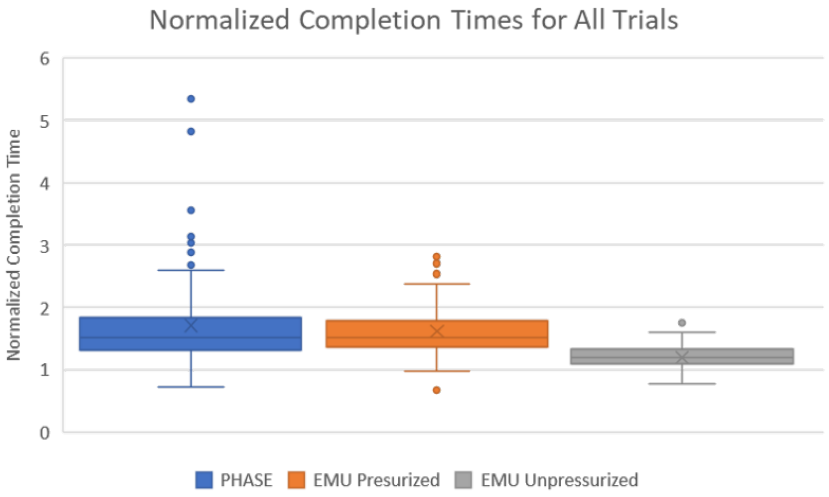

Figure 5.11: Normalized time required to complete one test for each participant. Quartile ranges are shown, with an x denoting the average across all participants and outliers shown as single points.

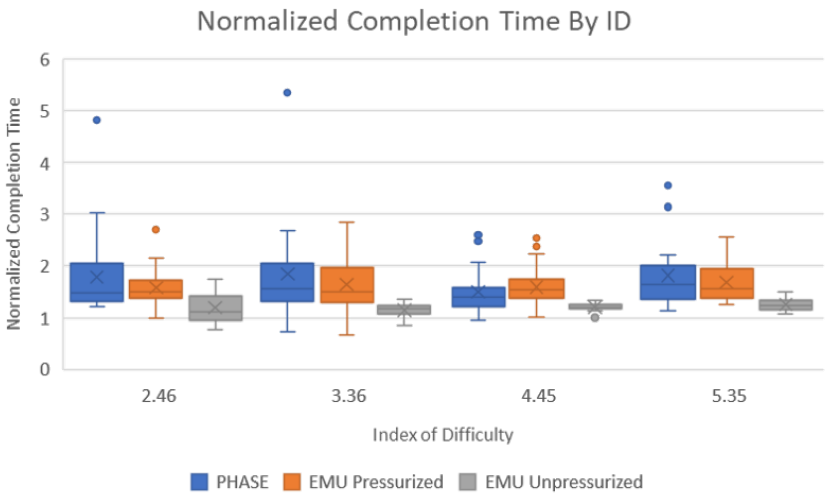

Figure 5.12: Normalized time required to complete a test at a given Index of Difficultyfor each participant. Quartile ranges are shown, with an x denoting the average across all participants and outliers shown as single points.

The results are consistent with the Fitts' Law analysis, showing that the PHASE arm required slightly more time to complete the tests, on average, than the pressurized EMU, with the exception of the trials that had an Index of Difficulty of 4.45. It is unclear why the PHASE arm seemed to slightly outperform the EMU in this particular trial. The unpressurized EMU test results were similar to the unsuited tests. Note that the unsuited tests are excluded from these graphs as they are, by definition, equal to 1.

Noteworthy in both the Fitts' Law and elapsed time analyses was the significant decline in performance between the unpressurized and pressurized EMU trials. This is an expected characteristic of soft suits that should be reduced by employing a rigid-element, constant volume design. PHASE was not pressurized for these trials, however, an ideal constant volume suit should be no more difficult to use pressurized than unpressurized. The increased friction associated with pressurization will affect

primarily k_1, therefore, it is expected that a pressurized PHASE prototype should also outperform a pressurized EMU at high Indices of Difficulty.

5.4.3 Participant Surveys

The PHASE arm scored slightly lower than the pressurized EMU arm for overall comfort (Figures 5.13 and 5.14). The difference in comfort can be addressed by including a comfort layer in the PHASE arm, which would minimize pinch-points and rubbing. The PHASE arm scored lower on ease of movement measures, which was expected, as the movement of the PHASE arm is not entirely natural and takes a while to adjust to. The PHASE arm and pressurized EMU arm rated equally for control and ease of extension. Most importantly, however, the PHASE arm scored lower than the EMU pressurized arm for the level of fatigue following task performance.

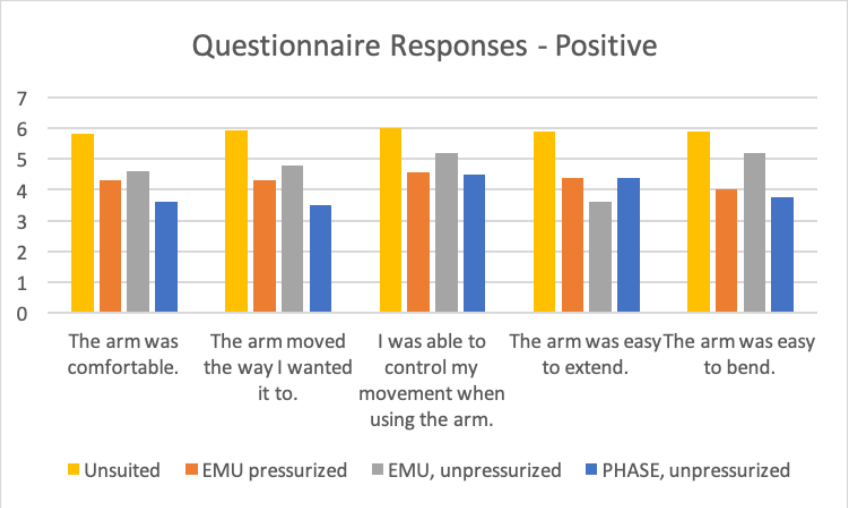

Figure 5.13: Average responses to questionnaire, where a higher score indicates a more positive result.

According to the Task Load Index, the PHASE arm was scored as more de-

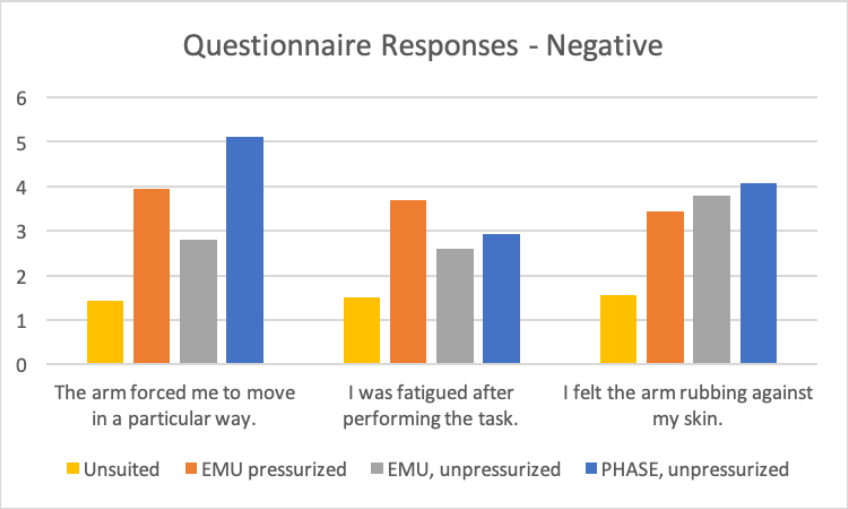

Figure 5.14: Average responses to questionnaire questions, where a higher score indicates a more negative result.

manding on the user than the pressurized EMU arm, though only marginally so (Figure 5.15). However, perceptions of success were nearly the same (Figure 5.16). The PHASE arm scored higher on the Cooper-Harper flowchart, as seen in Figure 5.17, again reflecting the learning curve associated with understanding how to manipulate the arm. Lastly, subjects were asked to identify points of discomfort, if any. Consistently, subjects noted the wrist and shoulder joints as points of discomfort. This discomfort is a function of the interfaces with the glovebox and wrist disconnect, neither of which are issues specific to the prototype. These concerns would not be present in a fully AM spacesuit, which would not require this interface. In the meantime, however, they can easily be addressed by including a comfort layer.

The PHASE arm scored worse than the pressurized EMU arm for most metrics in the participant surveys. However, most of these faults can be addressed with simple modifications of the PHASE design. Specifically, including a comfort layer that would protect the user from the rubbing and pinching that subjects noted in

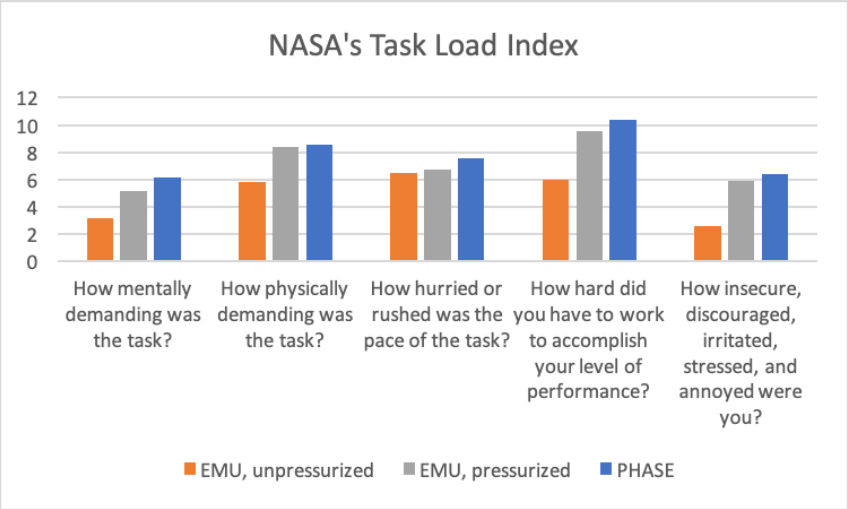

Figure 5.15: Average scores on NASA's Task Load Index.

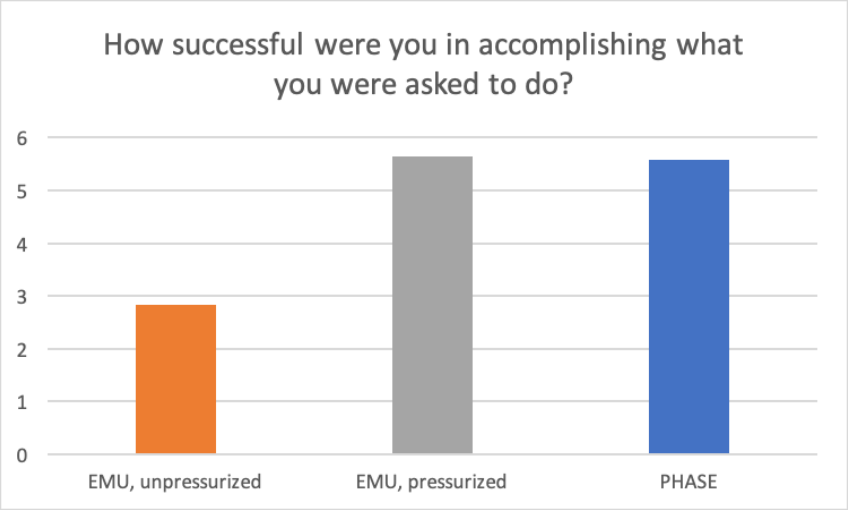

Figure 5.16: Average scores from NASA's Task Load Index question regarding perceived success in completion of the task.

their qualitative feedback. Additionally, the majority of the control issues are solved given more time to get acquainted with the kinematics of the PHASE arm.

Fatigue after use is a metric of interest, as it cannot be solved with a comfort layer or additional training. In this metric, the PHASE arm outperforms the EMU arm, which suggests that an AM hard suit can address some of the major concerns associated with current spacesuits.

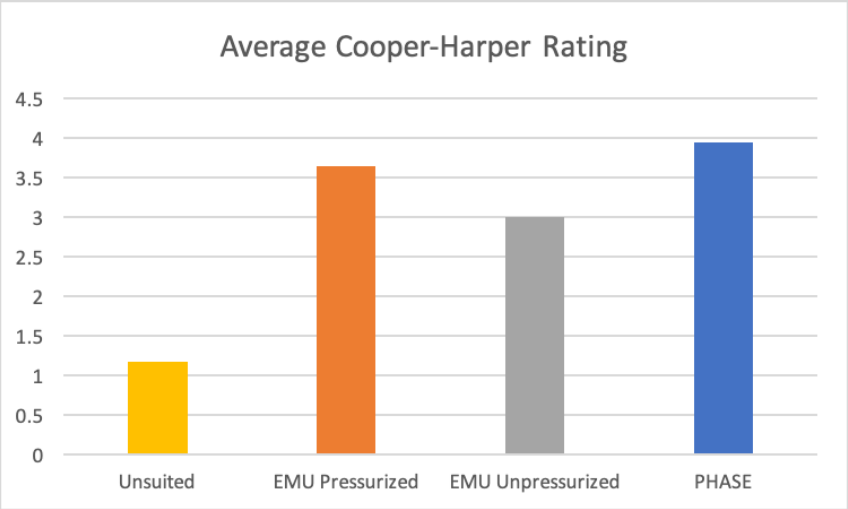

Figure 5.17: Average Cooper-Harper Handling Quality flowchart scores.

5.4.4 Sources of Error

Due to continued challenges in achieving the necessary tolerances for rotary seals using additively manufactured components, the PHASE arm was not pressurized during initial evaluation in the glovebox. This lack of pressurization may have improved the usability of the PHASE arm by reducing axial loads on the ball bearings and, therefore, the friction generated by the rotating wedge elements. PHASE's constant-volume design, however, is designed to minimize the effects of pressure differential on mobility by eliminating the presence of a single neutral position, as in the EMU arm. Constant-volume suits are expected to have a lower decline in performance in pressurized tests versus unpressurized, as compared to a traditional soft suit. As a result, the unpressurized PHASE arm is expected to demonstrate similar mobility characteristics to a pressurized PHASE arm. Therefore, the comparison between an unpressurized PHASE and pressurized EMU still provides meaningful data.

The silicone rubber glove used for pressurized testing cannot be worn unpressurized due to sizing constraints and the risk of damage to the glove created by its uninflated pressure bladder. As a result, a stand-in, unpressurized glove was fitted to the PHASE arm for unpressurized testing, while the silicone rubber glove was used for pressurized EMU tests. This glove lacked the silicone rubber pressure bladder, and as a result permitted more wrist flexibility. A greater portion of the motion analyzed by the Fitts' test could have been accomplished by moving only the wrist in the PHASE as compared to the EMU as a result. Participants were instructed to minimize the use of their wrist to complete the tapping task, and an 80 degree tapping arc was also evaluated to help mitigate the effects of the different gloves on mobility evaluations. Upcoming tests with the PHASE arm pressurized will allow both arms to use the same gloves, eliminating this potential error source.

5.5 Future Work

While this paper has discussed results to date on this project, at the current time a wealth of possible future directions are apparent. In the near term, the team will endeavor to complete the current data collection by getting pressurized data on the PHASE prototype. While a major source of leakage was identified in the physical connection to the glovebox, additional leaks were discovered in the rotary bearings themselves. Additional efforts to pinpoint the locations of these leaks and modify the existing bearings to provide adequate seals are ongoing. Additionally, traditional machining techniques can be used in conjunction with additive manufacturing in

future iterations, providing higher precision and likely improving the quality of the 3D-printed sealing surfaces.

At the end of this academic year, the Gemstone group "Team SPACE" who formed the core of this team will be graduating, and the continued development and testing of the hard suit concept will reside in the UMd Space Systems Laboratory (SSL). In parallel with the activities described here, the SSL has been developing a series of different kinematic configurations for wedge-based hardsuit arms, and testing them in unpressurized applications. The pioneering work of the Gemstone team will be the basis for the addition of pressurized suit elements to the ongoing SSL research.

There are several research projects that have been deferred to focus on the human testing described here. The team designed a single degree-of-freedom robotic system which can be inserted into a pressurized suit arm and directly measure the torque required for motion. This system would provide better data than the "traditional" approach of externally actuating an empty pressurized arm with a force gauge, particularly in its ability to record torque versus displacement as a function of velocity. The team also created a test rig to perform life testing on the additive manufactured bearings and seals, which will require a moderate redesign prior to operation. Ultimately that data will be critical before assessing the potential of this approach to the development of full pressure suits for human testing on Earth, and eventually in space.

5.6 Conclusion

The PHASE prototype successfully demonstrated that plastics fabricated using an SLS additive manufacturing process are able to withstand the loads and kinematic requirements for a rigid element spacesuit. PHASE successfully replicated the kinematics of the AX-5 suit at a lower mass, and with a higher potential for in-situ fabrication.

Future research should be conducted to investigate the in-situ production of spacesuits and spacesuit components based on the successes and lessons learned from the PHASE prototype. By investigating additional suit components and 3D-printed materials that have already been used on spacecraft, like Windform XT, the potential for the use of additive manufacturing to fabricate spacesuit components can be better understood. Furthermore, as additive manufacturing technology advances, many of the obstacles identified in the PHASE prototype may be mitigated, further increasing the potential uses of additive manufacturing in spacesuit production.

In particular, further research needs to be done on high-precision printing techniques that can support the smooth surface finish needed for additively manufactured sealing surfaces and bearings, as well as whether additive manufacturing can be used to fabricate seals and ball bearings. Additionally, research is needed on which additive manufacturing techniques can be used in reduced or zero gravity environments. FDM printing is currently the only technique that has been used in space; however, our research indicated that untreated FDM products do not seal and do not meet the precision requirements for rotary seals.

While the full potential for using additive manufacturing for in-situ spacesuit fabrication is not yet well understood, the PHASE prototype demonstrates that this is a technology worthy of further investigation while planning for long-duration human spaceflight missions.

Chapter 6: Final Discussion

Current space suit designs are incompatible with increased surface stay times required for human exploration of the Moon and Mars, bolstering the need for innovative technologies in the field of spacesuit manufacturing. This thesis has thoroughly discussed the first steps towards developing hard suit technologies which satisfy the stringent requirements associated with long-term human planetary settlement.

The present efforts have involved the design, fabrication, and test of a rigid spacesuit arm opposing the conventional wisdom of fabric "soft-good" used in current mission representative designs. A range of pneumatic, tensile, and 4-point bending tests were conducted to candidate 3D-printed materials with an eye to identifying top-candidate elements for the prototype. Based on these tests, it was found that SLS-fabricated materials were most promising for the fabrication of AM spacesuits, and thus the prototype was developed using DuraForm PA.

The PHASE prototype successfully replicated the kinematics of the AX-5, using a set of AM truncated spherical wedges and ball bearings. In the PHASE prototype, only the seals and metal bearings were not additively manufactured. While further research into AM seals and sealed bearings is required, the PHASE

prototype successfully replicated all other aspects of the AX-5 design, while reducing the design's mass and increasing the potential for in-situ fabrication.

The PHASE prototype did not fully demonstrate a 3D-printed, pressurized, hard spacesuit arm, however, it served as an effective proof of concept for the use of 3D printing in spacesuit fabrication. With the extended logistics cycles inherent to human Mars exploration, independence from Earth is crucial for mission success. Additive manufacturing, both for spacesuit components and for other aspects of space exploration, is a promising means of achieving this goal.

References

[1] S. J. Hoffman, "Advanced EVA Capabilities: A Study for NASA's Revolutionary Aerospace Systems Concept Program," Apr. 2004. [Online]. Available: https://ston.jsc.nasa.gov/collections/TRS/_techrep/TP-2004-212068.pdf

[2] N. C. Jordan, J. H. Saleh, and D. J. Newman, "The extravehicular mobility unit: A review of environment, requirements, and design changes in the US spacesuit," *Acta Astronautica*, vol. 59, no. 12, pp. 1135–1145, Dec. 2006. [Online]. Available: http://www.sciencedirect.com/science/article/pii/S0094576506001834

[3] V. E. Panfilov and V. S. Gurfinkel, "Biomechanical profile of the human-spacesuit interaction," *Human Physiology*, vol. 39, no. 7, pp. 750–755, Dec. 2013.

[4] "Alexei A. Leonov Inductee Profile." [Online]. Available: http://www.nmspacemuseum.org/halloffame/detail.php?id=17

[5] H. R. Griswold and J. D. Nash, "Working in a Shuttle EMU," in *Technology for Space Astrophysics*. American Institute of Aeronautics and Astronautics, 1982. [Online]. Available: http://arc.aiaa.org.proxy-um.researchport.umd.edu/doi/pdf/10.2514/6.1982-1847

[6] J. W. Wilson, J. Tweed, C. Zeitlin, M.-H. Kim, B. Anderson, F. Cucinotta, J. Ware, and A. Persans, "Shuttle spacesuit: Fabric/lcvg model validation," in *31st International Conference on Environmental Systems*. SAE International, 2001.

[7] M. L. Gernhardt, J. A. Jones, R. A. Scheuring, A. F. Abercromby, J. A. Tuxhorn, and J. R. Norcross, "Risk of Compromised EVA Performance and Crew Health Due to Inadequate EVA Suit Systems." [Online]. Available: https://humanresearchroadmap.nasa.gov/Evidence/reports/eva%20suit.pdf

[8] D. Akin, "Overview of current spacesuit engineering," Oct. 2016.

[9] M. M. S. Mousavi, A. Favetto, F. C. Chen, E. Ambrosio, S. Appendino, D. Manfredi, F. Pescarmona, and A. Soma, "Spacesuits and EVA Gloves Evolution and Future Trends of Extravehicular Activity Gloves," in *International Conference*

on Environmental Systems (ICES), Portland, Oregon, Jul. 2011. [Online]. Available: http://porto.polito.it/2460635/1/2011_Mousavi_Spacesuits_and_EVA_Gloves_Evolution_and_Future_Trends_of_Extravehicular_Activity_Gloves.pdf

[10] Kengo Ikema, A. V. Gubarevich, and O. Odawara, "Pneumatic Joint Design for Enhancing Spacesuit Flexibility," *Journal of Aerospace Engineering*, vol. 27, no. 2, pp. 347–353, Mar. 2014.

[11] P. Schmidt, "An investigation of space suit mobility with applications to EVA operations," Doctoral dissertation, Massachusetts Institute of Technology, Aug. 2001.

[12] J. A. Main, S. W. Peterson, and A. M. Strauss, "Design and structural analysis of highly mobile space suits and gloves," *Journal of Spacecraft and Rockets*, vol. 31, no. 6, pp. 1115–1122, 1994. [Online]. Available: http://dx.doi.org/10.2514/3.26567

[13] H. C. Vykukal, "Elbow and knee joint for hard space suits," U.S. Patent 4,598,427, Jul., 1986. [Online]. Available: https://ntrs.nasa.gov/search.jsp?R=19860019147

[14] D. L. Akin and K. Davis, "Hard Suits/Soft Suits: Revisiting Technologies and Applications for a New Space Era," in *45th International Conference on Environmental Systems*, Bellevue, Washington, Jul. 2015. [Online]. Available: https://ttu-ir.tdl.org/handle/2346/64515

[15] P. Dudek, "FDM 3d printing technology in manufacturing composite elements," *Archives of Metallurgy and Materials*, vol. 58, no. 4, pp. 1415–1418, 2013.

[16] R. Singh, "Process capability study of polyjet printing for plastic components," *Journal of Mechanical Science and Technology*, vol. 25, no. 4, pp. 1011–1015, Apr. 2011. [Online]. Available: https://doi.org/10.1007/s12206-011-0203-8

[17] D. Feeney, "FFF Vs. SLA Vs. SLS: 3d Printing," Aug. 2013. [Online]. Available: https://www.sd3d.com/fff-vs-sla-vs-sls/

[18] "Direct Metal Laser Sintering (DMLS)." [Online]. Available: https://www.stratasysdirect.com/technologies/direct-metal-laser-sintering

[19] R. R. MacKendrick and D. L. Finch, "Pressure sealing bearing assembly for use in environmental control suits and environmental suits containing such bearing assemblies," US Patent US4 596 054A, Jun., 1986. [Online]. Available: https://patents.google.com/patent/US4596054A/en

[20] "Pressure-Energized Seals," Nov. 2002. [Online]. Available: https://www.machinedesign.com/basics-design/pressure-energized-seals

[21] "Parker X-Ring Seals." [Online]. Available: https://www.parker.com/literature/O-Ring%20Division%20Literature/Bulletin%20pdf's/xring.pdf

[22] "Seal Design Guide." [Online]. Available: https://www.applerubber.com/src/pdf/seal-design-guide.pdf

[23] URS Corporation, "Development of an EVA systems cost model. Volume 1: Design guides synopsis-EVA equipment," NASA, Houston, TX, Technical Report NASA-CR-141634, Jul. 1974.

[24] J. E. Matty and L. Aitchison, "A Method for and Issues Associated with the Determination of Space Suit Joint Requirements," in *39th International Conference on Environmental Systems*. SAE International, 2009. [Online]. Available: http://dx.doi.org/10.4271/2009-01-2537

[25] "PolyJet Materials Data Sheet." [Online]. Available: http://usglobalimages.stratasys.com/Main/Files/Material_Spec_Sheets/MSS_PJ_PJMaterialsDataSheet.pdf?v=635785205440671440

[26] H. Bartlett, J. Bowser, C. C. Hierro, S. Garner, L. Guloy, C. Hnatov, J. Kalman, B. Sosis, and D. Akin, "In-Situ Fabricated Space Suits for Extended Exploration and Settlement," in *47th International Conference on Environmental Systems*, Jul. 2017. [Online]. Available: https://ttu-ir.tdl.org/handle/2346/73066

[27] N. J. C. S. D. , "Apollo Operations Handbook Extravehicular Mobility Unit," Mar. 1971. [Online]. Available: https://www.hq.nasa.gov/alsj/alsj-EMU1.pdf

[28] S. Garner, L. Carpenter, and D. Akin, "Developing Technologies and Techniques for Additive Manufacturing of Spacesuit Bearings and Seals," in *48th International Conference on Environmental Systems*, Jul. 2018. [Online]. Available: https://ttu-ir.tdl.org/handle/2346/74196

[29] "SLS - Selective Laser Sintering," Accessed on 2019-03-09. [Online]. Available: http://www.buildparts.com/processes/sls

[30] Y. Guiard and H. B. Olafsdottir, "On the Measurement of Movement Difficulty in the Standard Approach to Fitts' Law," *PLoS ONE*, vol. 6, no. 10, pp. 1–15, Oct. 2011. [Online]. Available: http://search.ebscohost.com/login.aspx?direct=true&db=a9h&AN=73889760&site=ehost-live

[31] P. M. Fitts, "The Information Capacity of the Human Motor System in Controlling the Amplitude of Movement," *Journal of Experimental Psychology*, vol. 121, no. 3, pp. 262–269, 1992. [Online]. Available: http://www.cs.princeton.edu/courses/archive/fall08/cos436/FittsJEP1954.pdf

[32] C. W. Moore, A. D. Nimbarte, and S. Rajulu, "Kinematic compatibility between the body and a mock spacesuit during basic upper body motions," *International Journal of Industrial Ergonomics*, vol. 44, no. 5, pp. 739–746, Sep. 2014. [Online]. Available: http://search.ebscohost.com.proxy-um.researchport.umd.edu/login.aspx?direct=true&db=bth&AN=98851721&site=ehost-live

[33] A. P. Anderson and D. J. Newman, "Pressure sensing for in-suit measurement of space suited biomechanics," *Acta Astronautica*, vol. 115, pp. 218–225, Oct. 2015. [Online]. Available: http://www.sciencedirect.com/science/article/pii/S0094576515002076

[34] S. G. Hart and L. E. Staveland, "Development of nasa-tlx (task load index): Results of empirical and theoretical research," in *Advances in psychology*. Elsevier, 1988, vol. 52, pp. 139–183.

[35] G. E. Cooper and R. P. Harper Jr, "The use of pilot rating in the evaluation of aircraft handling qualities," Advisory Group for Aerospace Research and Development, Tech. Rep., 1969.